U.S. Department
of Transportation
Federal Railroad
Administration

Office of Research,
Development and Technology
Washington, DC 20590

Raking Impact Testing of Diesel Multiple Unit (DMU) Fuel Tanks

DOT/FRA/ORD-21/33

Final Report | October 2021

NOTICE

This document is disseminated under the sponsorship of the Department of Transportation in the interest of information exchange. The United States Government assumes no liability for its contents or use thereof. Any opinions, findings and conclusions, or recommendations expressed in this material do not necessarily reflect the views or policies of the United States Government, nor does mention of trade names, commercial products, or organizations imply endorsement by the United States Government. The United States Government assumes no liability for the content or use of the material contained in this document.

NOTICE

The United States Government does not endorse products or manufacturers. Trade or manufacturers' names appear herein solely because they are considered essential to the objective of this report.

REPORT DOCUMENTATION PAGE

Form Approved
OMB No. 0704-0188

1. REPORT DATE *(DD-MM-YYYY)*	**2. REPORT TYPE**	**3. DATES COVERED** *(From - To)*
	Technical Report	September 2017–April 2020

4. TITLE AND SUBTITLE
Raking Impact Testing of Diesel Multiple Unit (DMU) Fuel Tanks

5a. CONTRACT NUMBER
DTFR5311D00008L

5b. GRANT NUMBER

5c. PROGRAM ELEMENT NUMBER

6. AUTHOR(S)
Travis Gorhum, 0000-0002-3088-9096
Michael Carolan, 0000-0002-8758-5739
Karina Jacobsen 0000-0002-3985-7349
Przemyslaw Rakoczy, 0000-0002-1924-7172
Melissa Shurland, 0000-0002-9055-6584

5d. PROJECT NUMBER
51RR28A400

5e. TASK NUMBER
DTFR5317F00783

5f. WORK UNIT NUMBER

7. PERFORMING ORGANIZATION NAME(S) AND ADDRESS(ES)
Transportation Technology Center, Inc., 55500 DOT Road, Pueblo, CO 81001
Volpe National Transportation Systems Center, 55 Broadway, Cambridge, MA 02142

8. PERFORMING ORGANIZATION REPORT NUMBER

9. SPONSORING/MONITORING AGENCY NAME(S) AND ADDRESS(ES)
U.S. Department of Transportation
Federal Railroad Administration
Office of Research, Development and Technology
Washington, DC 20590

10. SPONSOR/MONITOR'S ACRONYM(S)

11. SPONSOR/MONITOR'S REPORT NUMBER(S)
DOT/FRA/ORD-21/33

12. DISTRIBUTION/AVAILABILITY STATEMENT
This document is available to the public through the FRA website.

13. SUPPLEMENTARY NOTES
COR: Melissa Shurland

14. ABSTRACT
On December 18, 2018, a quasi-static raking test of a diesel multiple unit (DMU) fuel tank was conducted at the Transportation Technology Center (TTC) in Pueblo, CO. This test resulted in puncture of the tank's end sheet and a 22.6-inch tear in its bottom sheet. On November 13, 2019, a second quasi-static raking test of a DMU fuel tank was conducted, which scraped the tank's bottom sheet for 44.6 inches and produced two distinct puncture locations. A finite element (FE) model was developed of the fuel tank and indenter to prepare for the raking tests. Overall, both the pre- and post-test FE models exhibited limited agreement with the test measurements up to the point of material failure, when the fuel tank begins to tear.

15. SUBJECT TERMS
Diesel multiple unit fuel tanks, impact test, crashworthiness, finite element analysis, puncture resistance, DMU, passenger locomotive, fuel tanks, raking, rolling stock

16. SECURITY CLASSIFICATION OF:			**17. LIMITATION OF ABSTRACT**	**18. NUMBER OF PAGES**	**19a. NAME OF RESPONSIBLE PERSON**
a. REPORT	**b. ABSTRACT**	**c. THIS PAGE**			Travis Gorhum, Sr. Engineer
Unclassified	**Unclassified**	**Unclassified**		72	**19b. TELEPHONE NUMBER (Include area code)** 719-584-0720

Standard Form 298 (Rev. 8/98)
Prescribed by ANSI Std. Z39.18

METRIC/ENGLISH CONVERSION FACTORS

ENGLISH TO METRIC

LENGTH (APPROXIMATE)

1 inch (in)	=	2.5 centimeters (cm)
1 foot (ft)	=	30 centimeters (cm)
1 yard (yd)	=	0.9 meter (m)
1 mile (mi)	=	1.6 kilometers (km)

AREA (APPROXIMATE)

1 square inch (sq in, in^2)	=	6.5 square centimeters (cm^2)
1 square foot (sq ft, ft^2)	=	0.09 square meter (m^2)
1 square yard (sq yd, yd^2)	=	0.8 square meter (m^2)
1 square mile (sq mi, mi^2)	=	2.6 square kilometers (km^2)
1 acre = 0.4 hectare (he)	=	4,000 square meters (m^2)

MASS - WEIGHT (APPROXIMATE)

1 ounce (oz)	=	28 grams (gm)
1 pound (lb)	=	0.45 kilogram (kg)
1 short ton = 2,000 pounds (lb)	=	0.9 tonne (t)

VOLUME (APPROXIMATE)

1 teaspoon (tsp)	=	5 milliliters (ml)
1 tablespoon (tbsp)	=	15 milliliters (ml)
1 fluid ounce (fl oz)	=	30 milliliters (ml)
1 cup (c)	=	0.24 liter (l)
1 pint (pt)	=	0.47 liter (l)
1 quart (qt)	=	0.96 liter (l)
1 gallon (gal)	=	3.8 liters (l)
1 cubic foot (cu ft, ft^3)	=	0.03 cubic meter (m^3)
1 cubic yard (cu yd, yd^3)	=	0.76 cubic meter (m^3)

TEMPERATURE (EXACT)

[(x-32)(5/9)] °F = y °C

METRIC TO ENGLISH

LENGTH (APPROXIMATE)

1 millimeter (mm)	=	0.04 inch (in)
1 centimeter (cm)	=	0.4 inch (in)
1 meter (m)	=	3.3 feet (ft)
1 meter (m)	=	1.1 yards (yd)
1 kilometer (km)	=	0.6 mile (mi)

AREA (APPROXIMATE)

1 square centimeter (cm^2)	=	0.16 square inch (sq in, in^2)
1 square meter (m^2)	=	1.2 square yards (sq yd, yd^2)
1 square kilometer (km^2)	=	0.4 square mile (sq mi, mi^2)
10,000 square meters (m^2)	=	1 hectare (ha) = 2.5 acres

MASS - WEIGHT (APPROXIMATE)

1 gram (gm)	=	0.036 ounce (oz)
1 kilogram (kg)	=	2.2 pounds (lb)
1 tonne (t)	=	1,000 kilograms (kg)
	=	1.1 short tons

VOLUME (APPROXIMATE)

1 milliliter (ml)	=	0.03 fluid ounce (fl oz)
1 liter (l)	=	2.1 pints (pt)
1 liter (l)	=	1.06 quarts (qt)
1 liter (l)	=	0.26 gallon (gal)
1 cubic meter (m^3)	=	36 cubic feet (cu ft, ft^3)
1 cubic meter (m^3)	=	1.3 cubic yards (cu yd, yd^3)

TEMPERATURE (EXACT)

[(9/5) y + 32] °C = x °F

QUICK INCH - CENTIMETER LENGTH CONVERSION

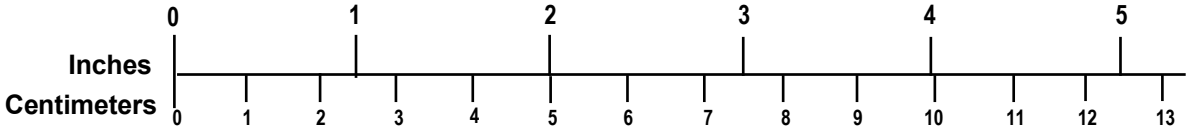

QUICK FAHRENHEIT - CELSIUS TEMPERATURE CONVERSIO

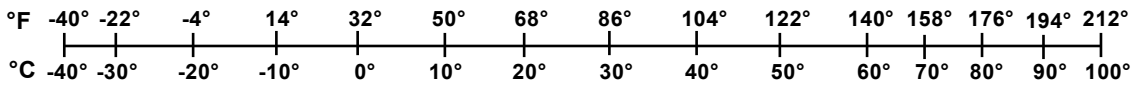

For more exact and or other conversion factors, see NIST Miscellaneous Publication 286, Units of Weights and Measures. Price $2.50 SD Catalog No. C13 10286

Updated 6/17/98

Acknowledgements

The Volpe National Transportation Systems Center's authors are grateful for the cooperation of the diesel multiple unit (DMU) manufacturer in providing detailed information on tank construction, and design and installation hardware in support of the testing. They also gratefully acknowledge the contributions of their colleague Dr. A. Benjamin Perlman for his invaluable advice in model development, validation, and test design.

Transportation Technology Center, Inc.'s authors acknowledge the contributions of their test and support team: Mitch Miller, Andrew Hawk, Bruce Perrin, and Justin Penrod.

Contents

Illustrations

Tables

Executive Summary

The Federal Railroad Administration's (FRA) Office of Research, Development and Technology is conducting research into passenger locomotive fuel tank crashworthiness. The Volpe National Transportation Systems Center (Volpe) supports FRA in evaluating the crashworthiness of fuel tank designs and developing technical research for supporting standard and regulation development. Researchers conducted a series of impact tests to measure fuel tank deformation under two types of dynamic loading conditions: blunt impact and raking impact. Test specimens included a set of FRA-owned retired passenger locomotive fuel tanks and a set of new diesel multiple unit (DMU) fuel tanks purchased by FRA from a manufacturer of DMU equipment currently in passenger rail operation in the United States.

On December 18, 2018, FRA contracted Transportation Technology Center, Inc. (TTCI) to conduct a quasi-static raking test of a DMU fuel tank at the Transportation Technology Center (TTC) in Pueblo, CO. TTCI developed specialized hardware and procedures for testing the DMU fuel tank which was mounted to the underframe structure of a boxcar. Researchers placed the boxcar in the squeeze fixture at the TTC. The squeeze fixture's hydraulic cylinders pushed the boxcar into a 3-foot long by 0.75-inch wide indenter mounted between the rails. This indenter was positioned against the fuel tank's end sheet with approximately 2 inches of overlap between the top of the indenter, and the bottom of the end sheet. The indenter punctured the tank's end sheet and tore into the bottom sheet for 22.6 inches, applying a maximum force of 51,000 pound-force (lbf).

On November 13, 2019, TTCI conducted a second quasi-static raking test of a DMU fuel tank. Researchers mounted the second fuel tank to the underframe structure of a boxcar, and then placed in the squeeze fixture at the TTC. During this test, the indenter was positioned against the fuel tank's sloped bottom sheet, bypassing the tank's end sheet. The squeeze fixture's hydraulic cylinders pushed the boxcar into the track mounted indenter used for the first test. The indenter scraped the surface of the fuel tank for 44.6 inches and produced two separate tears in the tank's bottom sheet. The maximum force was 21,000 lbf.

Volpe developed a finite element (FE) model of the fuel tank and indenter that was used in preparation for the raking tests. The pre-test model used material properties and failure criterion developed for the previous blunt impact test and modeling effort [1]. Overall, both the pre- and post-test FE models exhibited limited agreement with the raking test results up to the point of material failure, when the fuel tank begins to tear.

1. Introduction

The Federal Railroad Administration (FRA) contracted with Transportation Technology Center, Inc. (TTCI) to conduct a series of impact tests to evaluate the performance of passenger locomotive fuel tanks under dynamic loads. Researchers conducted these tests between September 25, 2017, to March 31, 2020. FRA conducted the fuel tank research to support the development of strategies for increasing passenger locomotive fuel tank puncture resistance to mitigate the risk of a post-collision or post-derailment fire. In accidents, fuel tanks can experience dynamic loading often consisting of a blunt or raking impact from various components of the rolling stock or trackbed [1]. Current design standards require that fuel tanks have properties adequate to sustain a prescribed set of minimum static load conditions. The intent of the research described here is to increase the understanding of the structural response of fuel tanks under dynamic loading. By utilizing an approach that has been effective in evaluating the structural crashworthiness of passenger railcars, improved strategies can be developed that will address the types of loading conditions observed in collisions or derailment events.

A series of raking impact tests on diesel multiple unit (DMU) fuel tanks took place at the Transportation Technology Center (TTC), in Pueblo, CO. Detailed finite element analysis (FEA) models developed by the Volpe National Transportation Systems Center (Volpe) were used to estimate the behavior of the tanks during raking, prior to testing. Test results were used to improve the FE models and aided in evaluating the accuracy of pre-test analysis. This report describes the first and second raking tests of DMU fuel tanks and the corresponding FEA.

1.1 Background

Passenger fuel tank crashworthiness research is conducted as part of FRA's Train Occupant Protection Research Program. Previous research investigated passenger train fuel tank crashworthiness during dynamic blunt impacts [2][3]. DMU fuel tanks are smaller than conventional passenger locomotive fuel tanks but are required to meet the same regulations.

Researchers conducted a survey as part of the research effort on accidents and derailments in the U.S. over the last two decades in which fuel tanks were punctured [1]. The survey findings on such incidents were obtained using a combination of the FRA accident database and in-person field investigations conducted by FRA inspectors and support staff from Volpe. The surveys consisted of freight and passenger trains involved in accidents or derailments during which one or more fuel tanks ruptured. There were two key findings identified from the results of this survey. First, a fuel tank rupture during a train collision or derailment may result in a fire, which presents additional threats to the survivability of passengers and crew as they egress from the collision wreckage. For passenger operations that utilize DMUs, the risk associated with a diesel spill, fire, and injuries and/or fatalities is higher with the presence of more people on board the consist and their proximity to the ejected fuel. The second key finding is that each fuel tank impact scenario can be categorized by its resultant loading type, of which there are two general loading conditions leading to punctures: blunt impacts and raking impacts.

The schematics in Figure 1 illustrate two idealized loading scenarios identified in this research that can penetrate an exposed surface of a fuel tank. A "blunt" impact is characterized by a rigid object aligned relative to a fuel tank such that it imparts a primarily perpendicular force to the fuel tank surface. A "raking" impact is characterized by a rigid object initially aligned such that it applies a primarily tangential force imparting a tearing load upon the fuel tank surface. Note

that a raking impact can rake along the side of the fuel tank, or along the bottom surface of the fuel tank with similar outcomes.

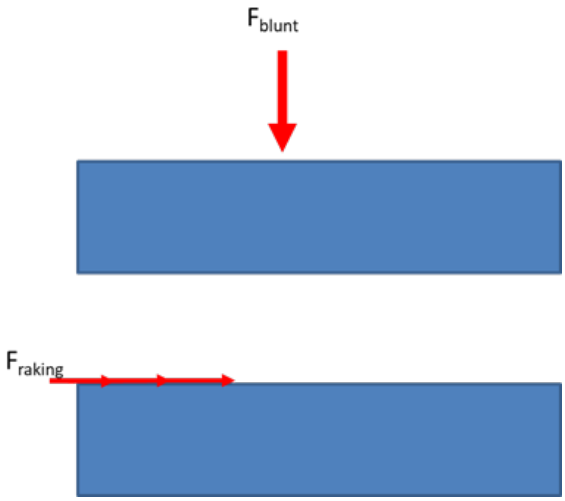

Figure 1. Force Diagrams of Fuel Tank Loading Types

This report describes the efforts to develop a raking impact test scenario. To highlight the raking load scenario, Figure 2 shows an incident from a rail yard in Newark, NJ, from April 2012. In this incident, two locomotives impacted the side of another train at a switch. Through the sequence of events, a doortrack of the trailing freight car was dragged along the side of the lead locomotive fuel tank. Figure 3 shows the resulting damage to the fuel tank.

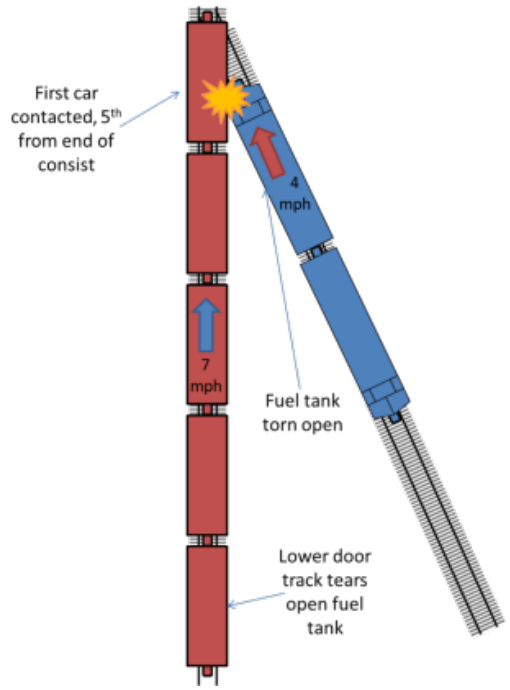

Figure 2. Schematic of Raking Impact in Oak Island Yard in Newark, NJ

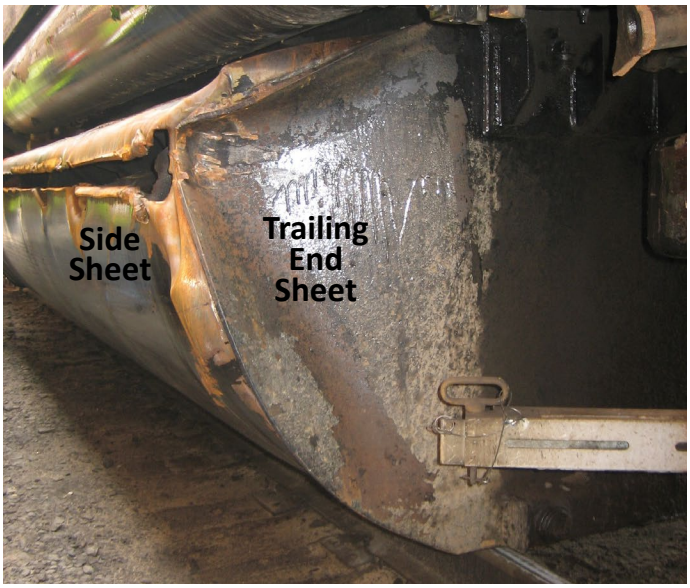

Figure 3. Damage to Lead Locomotive Fuel Tank

FRA sponsored a series of full-scale tests to evaluate fuel tanks under blunt and raking impact loading scenarios. In the first phase, researchers designed and used the test setup for blunt impact to test three retired passenger locomotive fuel tanks and one DMU fuel tank. The total weight of the impact vehicle with the 12-inch by 12-inch square indenter was 14,075 pounds. The first two tests were performed on conventional passenger locomotive fuel tanks on October 2013 and August 2014 at low speeds: 4.5 and 6.2 mph, respectively. Researchers chose the targeted speeds to impart permanent deformation to the tank. The force-deflection characteristics of each impact were measured [3][4][5][6][7][8]. These tests provided valuable initial information on the variance of tank performance based on design details.

A third test took place on August 20, 2014, with an identical test setup, on a retired conventional passenger locomotive fuel tank, at 11.2 mph. A fourth test took place on June 28, 2016, on a DMU fuel tank at 11.1 mph. The objectives of these tests were to measure the performance of conventional fuel tanks and DMU fuel tanks under a dynamic blunt impact [2][4][9]. For this research, TTCI purchased new DMU fuel tanks from a DMU equipment manufacturer operating in the U.S. The conventional locomotive fuel tanks were repurposed from test locomotives owned by FRA and located at the TTC.

While the impact conditions of the third and fourth tests were nearly identical, the impact responses of the fuel tanks were very different. The details of the fuel tank internal baffle construction contributed to the progression of each tank's response to the load. Results of one of the blunt impact tests on a conventional fuel tank from an F40 locomotive (#234) featured a very low initial force after impact attributed to the gap between the interior of the bottom of the tank and the lateral baffles followed by a rise to the peak force. In contrast, the DMU fuel tank featured baffles that were spot-welded to the bottom sheet. The DMU fuel tank experienced a high initial force, while the conventional tanks did not experience a significant increase in stiffness until the bottom sheet closed the gap with the baffles. Both tanks experienced buckling of their baffles, which resulted in a temporary decrease in force.

Figure 4 shows the deformed shapes of the F40 and DMU fuel tanks. Because it was stiffer, the DMU fuel tank experienced much less deformation compared to the conventional fuel tank. However, because the DMU fuel tank had a smaller overall height than the conventional fuel tank, the maximum indentation as a percentage of the initial tank height experienced by the DMU tank was significantly more than the conventional tank.

Figure 4. Deformed Shapes of Tank 234 (left) and DMU Fuel Tank (right)

This test report describes the second phase of testing, which is the development of a raking load scenario. The report includes preparation, modeling, and results from two raking tests conducted on DMU fuel tanks.

1.2 Objectives

The key objective of the raking testing of fuel tanks was to examine the gross response of the fuel tanks to a given impact type. The purpose of the raking test design was to characterize each test specimen's deformation behavior when scraped along the bottom sheet, both with and without first engaging the end sheet.

The outcome of this process can be used to make a comparison between fuel tanks of different designs, with analysis techniques being used to provide additional information on the fuel tank behavior. Modeling can also be used to simulate additional impact conditions beyond what was tested, providing additional points of comparison between different designs.

1.3 Overall Approach

This research effort used FE modeling in conjunction with full-scale testing to better understand the behaviors of a DMU fuel tank under raking impact conditions. Prior to the tests, researchers used engineering drawings and computer-aided design (CAD) geometry to generate a detailed

FE mesh of the fuel tank. An estimation of material responses, including plastic stress-strain responses were made for the DMU fuel tanks' materials. Each pre-test FE model was used to plan for instrumentation range and placement, as well as to determine the location of raking along the fuel tank. Researchers compared the results of each test to the corresponding FE model. The overall approach to characterizing the deformation behavior included:

1. Development of an analytical model of the fuel tank specimen based upon known design details
    - Use the analytical model to plan for tests
    - Estimate possible fuel tank behavior under test impact conditions
2. Design test setup to apply desired load to fuel tank
    - Develop test setup for achieving desired load path and load application on fuel tank
    - Fabricate indenter
    - Develop and fabricate test fixture for indenter
    - Develop mounting scheme for fuel tank and modify boxcar
    - Perform pre-test checks on test setup to validate desired load path
3. Apply a scraping load to the bottom surface of a fuel tank specimen
    - Measure the force-deflection behavior of the tank with specified instrumentation
    - Record mode of deformation with conventional video cameras
    - Record permanent deformation by surface light detection and ranging (LIDAR) scans
4. Conduct post-test examination of the tank
    - Characterize structural deformation of tank exterior and interior
5. Validate the model
    - Compare test results to model predictions
    - Revise model as necessary

1.4 Scope

This report describes the test preparations, instrumentation, and the data collected from the two tests. It also includes a discussion of the development of the pre-test FE models and modifications to the model after the test to reflect measured differences in the fuel tank response.

1.5 Organization of the Report

This report is organized in the following six sections: Section 1 holds an introduction and describes the organization of the report. Section 2 describes the test setup for the raking impact tests conducted on two fuel tank specimens to date. Section 3 offers an overview of the computer simulation used to model the responses of the fuel tanks to the two raking impacts. Section 4 presents the results from the tests and the corresponding computer simulations, and compares these results to one another. Section 5 contains some concluding remarks and discussion about

the testing and analysis program. Appendices A and B provide test data from the first and second raking tests.

2. Test Requirements and Methods

This section describes the test setup and test procedure from the raking impact tests. The first raking test, conducted on December 18, 2018, assessed the adequacy of the test setup pertaining to the fixturing and arrangement of the test specimen and indenter, in addition to testing the behavior of the fuel tank. The second test, conducted on November 13, 2019, used a setup similar to the first test, except that the initial position of the indenter was adjusted to bypass the end sheet of the fuel tank.

2.1 Test Setup Design

Researchers conducted the DMU fuel tank raking tests in the squeeze fixture at the TTC. TTCI constructed a mounting structure for the fuel tanks which was rigidly attached underneath a boxcar at its center sill. This mounting structure consisted of five box beams welded to the boxcar's center sill. The research team welded reinforced c-channels built for the DMU blunt impact test to the box beams to provide a mounting structure for the fuel tank installation. The use of mounting hardware provided by the fuel tank manufacturer enabled the fuel tanks to be attached to this mounting structure: a 20 mm (0.787-inch) diameter bolt, rubber bushing, and set of washers. This mounting method created a support condition similar to how the fuel tanks would be installed on a DMU. Figure 5 shows the box beams, reinforced c-channels, and fuel tank mounted underneath the test boxcar.

Figure 5. Fuel Tank Mounting Structure

An indenter made of welded plate steel was mounted on the track structure beneath the boxcar and positioned at the point of first contact with the fuel tank. The purpose for the design of this indenter was to have roughly the same thickness as the web of a rail. This was selected to simulate the fuel tank being impacted by a broken rail. The construction of the indenter itself was of high strength A514 Grade B plate steel to resist deformation during the tests. Figure 6 shows the indenter in its configuration for Test 1

Figure 6**. Test 1 Indenter**

The placement of the indenter was placed within a baseplate mounted to a concrete pad in the squeeze fixture. The baseplate consisted of a few thick steel plates welded together that had L-brackets welded to it on the front, and bolt holes for a load cell support bracket at the back. The placement of the indenter was within the space created by the L-brackets and separated from the baseplate material by a liner made of polytetrafluoroethylene (PTFE). The PTFE liner had a low coefficient of friction, which prevented longitudinal force from being transmitted directly into the baseplate. At the rear of the baseplate was the load cell support bracket. This bracket was bolted into the baseplate, and held a load cell positioned against the back of the indenter during the test. The design of the setup of the indenter and baseplate was to allow the indenter load cell to measure as much of the longitudinal force being placed into the indenter as possible. The purpose of the setup of the indenter/baseplate combination was to minimize the load paths that could bypass the load cell and result in a smaller reading of the longitudinal force placed on the indenter. Figure 7 shows a photograph of the final arrangement of the indenter, baseplate, PTFE liner, load cell bracket, and load cell.

Figure 7. Indenter and Baseplate Setup

During these tests, the hydraulic cylinders in the squeeze fixture applied the load to a sled. This sled slides upon the lower set of longitudinal I-beams in the squeeze fixture and stabilizes the transfer of force from two hydraulic cylinders to the boxcar's center sill. The friction force between the sled and the I-beams is negligible due to low normal force on the sliding flanges. Researchers positioned a sled-mounted load cell to measure all the longitudinal force that was transmitted into the boxcar. The load is then transmitted through the boxcar sill and carbody structure into the box beams and c-channels that make up the fuel tank mounting structure. The load is further transmitted from the mounting structure into the DMU fuel tank, through the tank's mounting bolts and bushings. This load is then reacted by the indenter, which was mounted in the baseplate, and rigidly attached to a concrete pad in the squeeze fixture. The indenter load cell measured the reacted load. The use of the test setup was to minimize any other potential load paths such that force placed into the boxcar and measured by the boxcar load cell would match the force reacted by the indenter, which would be measured by the indenter load cell. Figure 8 illustrates this load path and Figure 9 depicts the overall test setup.

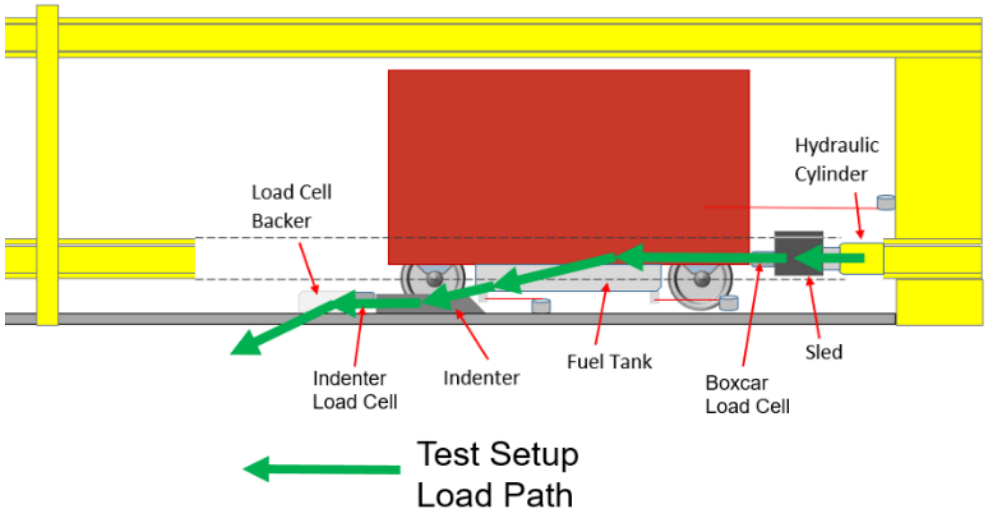

Figure 8. Primary Load Path

Figure 9. View of Boxcar in Test Fixture and View of Indenter Setup

2.2 Rolling Resistance Test

Prior to the first raking test, the work required a rolling resistance test on the boxcar. This test consisted of using the hydraulic cylinders in the squeeze fixture to push the boxcar without the indenter in place, allowing the boxcar to roll freely within the squeeze fixture. A load cell measured the force that was applied to the boxcar and determined the amount of force required to move the car. The maximum force measured during this test never exceeded 280 pound-force (lbf) and the data considered it negligible compared to the forces measured during the tests. Figure 10 shows the force measurement. Note that at certain points in this test, the force dropped to zero because the boxcar would occasionally roll away from the load cell when a force was applied.

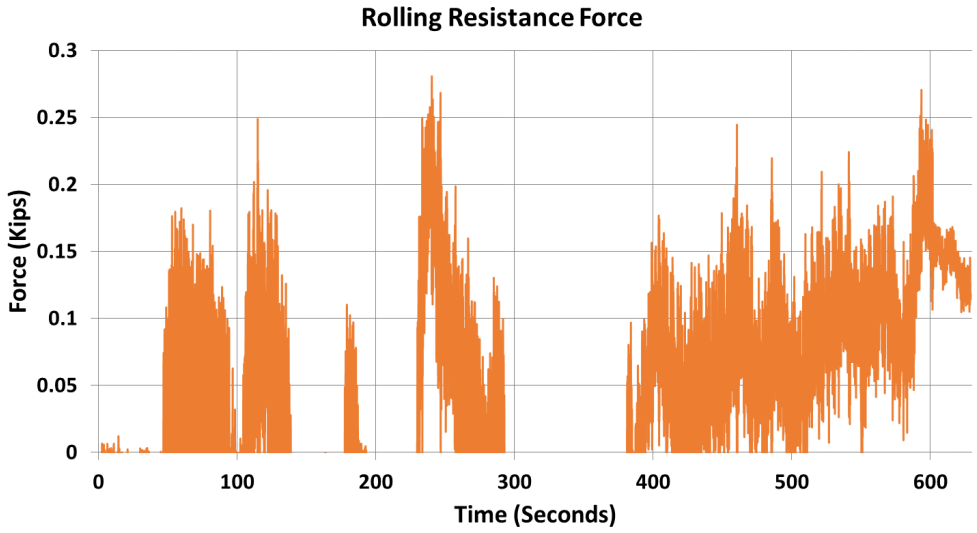

Figure 10. Rolling Resistance Force

2.3 Test 1 and Test 2 Setup

During the first test, researchers positioned the indenter against the fuel tank's end sheet with a 2-inch overlap between the top of the indenter and the bottom of the end sheet. The positioning of the indenter was so to rake along a weld seam running longitudinally on the bottom sheet of the fuel tank. To place the indenter at this weld seam, the indenter was offset 9.8 inches from the center of the fuel tank. Figure 11 shows the indenter location at the beginning of the first raking test.

Figure 11**. Test 1 Indenter Contact**

During the second test, the positioning of the indenter bypassed the fuel tank's end sheet to make first contact with the tank's bottom sheet. The positioning of the front of the indenter was roughly 18 inches past the tank's end sheet. During the second test, the indenter was offset roughly 4.8 inches from the center of the fuel tank, which allowed the indenter to rake the tank near an internal, longitudinal baffle. This lateral location was offset approximately 5 inches toward the center of the tank from the raking location for the first test. Figure 12 shows the indenter location at the beginning of the second raking test.

Figure 12. Test 2 Indenter Contact

2.4 Test 1 Methods

FRA, Volpe, and TTCI developed the test requirements. Use of the TTC squeeze fixture to impart a raking force onto a mounted DMU fuel tank had never been undertaken. The first raking test was the first time use of this particular test arrangement. Thus, researchers designed the first test to not only serve as a test of the DMU fuel tank, but also as a "shakedown" test of the new test setup. Since there was the potential for unexpected difficulties to arise, the first test did not use a brand new DMU fuel tank in the untested setup. Rather, the fuel tank used in this test was a DMU fuel tank that was previously tested in a blunt impact test [2]. As such, this fuel tank had significant plastic deformation on one end. However, the positioning of the tank was under the boxcar such that the undeformed end experienced the raking.

During this test, the boxcar supported the fuel tank underneath as described in Sections 2.1 and 2.3. Researchers installed the indenter on a concrete jacking pad between the rails in the squeeze fixture. The position of the leading edge of the indenter was against the end sheet of the fuel tank and aligned with a longitudinal weld seam in the bottom sheet of the fuel tank. Figure 13 shows the relative positions of the indenter and the fuel tank.

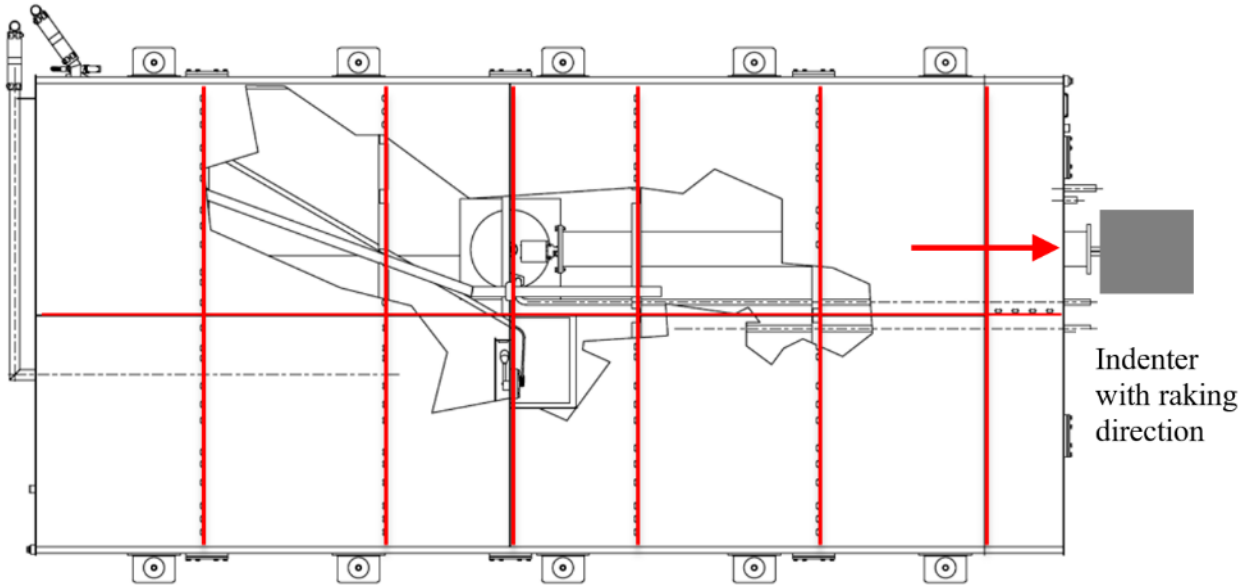

Figure 13. Top View of Test 1 DMU Fuel Tank (baffle locations in red) with Indenter Location and Raking Direction

During the test, the hydraulic cylinders in the squeeze fixture slowly pushed the boxcar with the attached fuel tank into the indenter. When the stroke of the cylinders was exhausted at approximately 11.8 inches, chocks were placed on the boxcar to secure it. The hydraulic cylinders were then retracted and a spacer was placed between the hydraulic cylinders and the boxcar to incrementally continue the longitudinal movement of the boxcar. The boxcar was pushed for two full strokes of the hydraulic cylinders. Data collected during the test included forces, pressures, displacements, and high definition video recordings.

2.5 Test 2 Methods

The tank used for Test 2 was a DMU fuel tank newly built to the same design as the DMU tank used in the first raking test.

During this test, the boxcar supported the fuel tank underneath it as described in Section 2.1 and the installation of the indenter took place on a concrete jacking pad between the rails in the squeeze fixture. In this test, however, the indenter was initially positioned underneath the fuel tank. The indenter's leading edge was inboard from the fuel tank end sheet by approximately 18 inches and the center of the indenter was shifted 5 inches toward the center of the fuel tank as measured from the longitudinal weld seam in the tank's bottom sheet. The front top edge of the indenter was in contact with a bottom sheet of the fuel tank, as the fuel tank featured a bottom sheet that sloped downward toward the center of the fuel tank. Figure 14 depicts the relative positions of the indenter and the fuel tank.

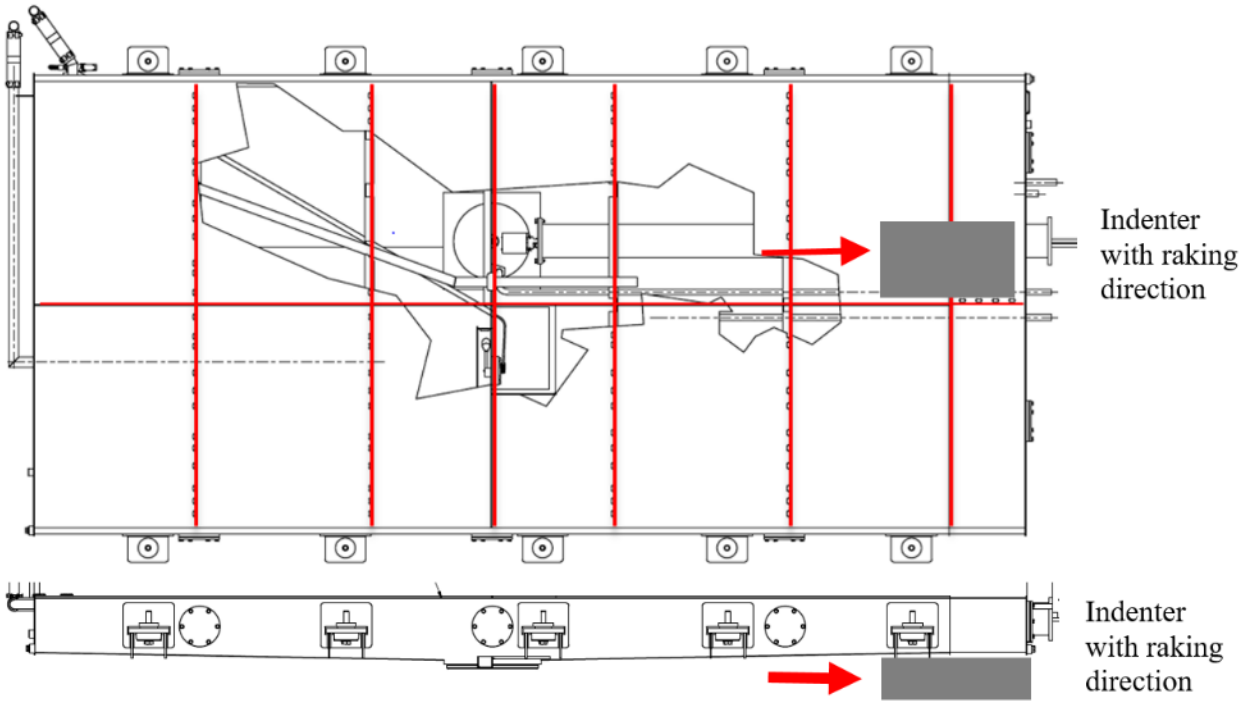

Figure 14. Top and Side Views of Test 2 DMU Fuel Tank with Indenter Location and Raking Direction

During test, the hydraulic cylinders in the squeeze fixture slowly pushed the boxcar with the attached fuel tank into the indenter. The fuel tank's bottom sheet sloped down toward the center of the tank, which increased the overlap distance between the tank and indenter as the boxcar was pushed. When the stroke of the cylinders was exhausted at approximately 11.8 inches, chocks were placed on the boxcar to secure it. The hydraulic cylinders were then retracted and added a spacer between the hydraulic cylinders and the boxcar to incrementally continue the longitudinal movement of the boxcar without a change in the force between the fuel tank and indenter. This process was repeated to push the boxcar for four full strokes of the hydraulic cylinders. Data collected during this test included forces, pressures, displacements, and high definition video recordings.

2.6 Test Instrumentation

The primary goal of the instrumentation was to measure the force applied to the DMU fuel tank and its travel distance across the indenter. Researchers used the same instrumentation arrangement in both raking tests, as described in this section.

2.6.1 Definition of Coordinate Axes

All local force and displacement coordinate systems are defined relative to the boxcar. Positive x, y, and z directions are forward, left, and up, respectively, relative to the raking direction.

2.6.2 Instrumentation Summary

The instrumentation used was identical for both raking tests. Table 1 summarizes the instrumentation count and type.

Table 1. Instrumentation Summary

Type of Instrumentation	Channel Count
String potentiometer	6
Load cells	2
Displacement from hydraulic cylinders	2
Pressure from hydraulic cylinders	2
Laser displacement	1
Total data channels	**13**
Digital video	3 cameras

2.6.3 Fuel Tank and Car Displacements

Researchers used four string potentiometers to measure the longitudinal displacement of the fuel tank, with one string potentiometer placed at each corner of the fuel tank. In addition, two string potentiometers measured the longitudinal displacement of the boxcar at the live end near the point of load application. Figure 15 and Figure 16 show the configuration of these displacement measurements. Table 2 lists the locations and ranges for the six string potentiometers. Using one laser displacement sensor allowed the measurement of the vertical displacement of the fuel tank. The laser sensor was directed at the fuel tank mounting structure, to provide a consistent reading for the full travel of the boxcar.

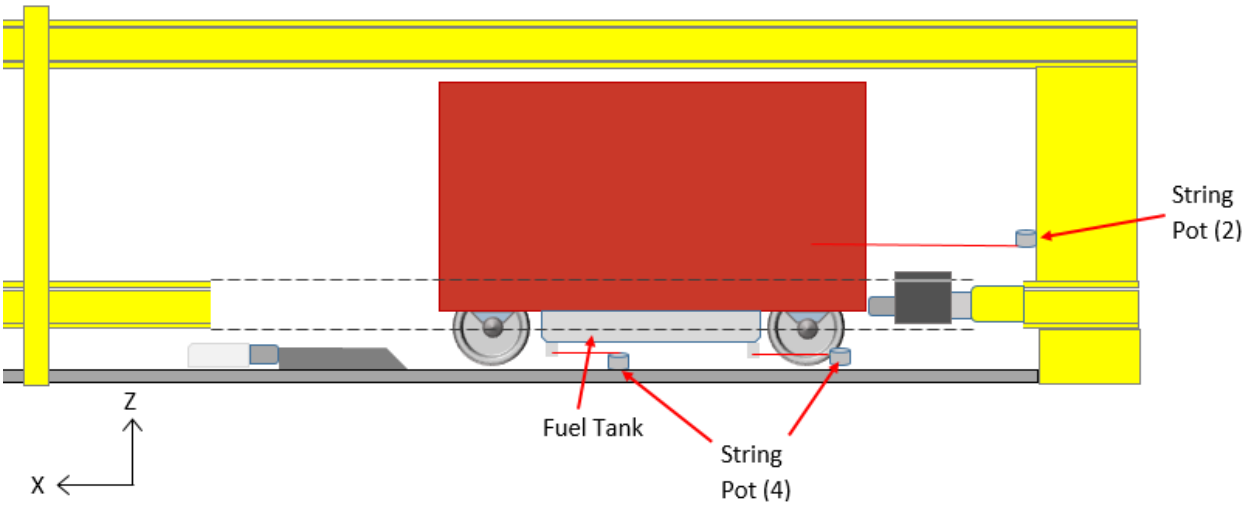

Figure 15. String Potentiometers (side view)

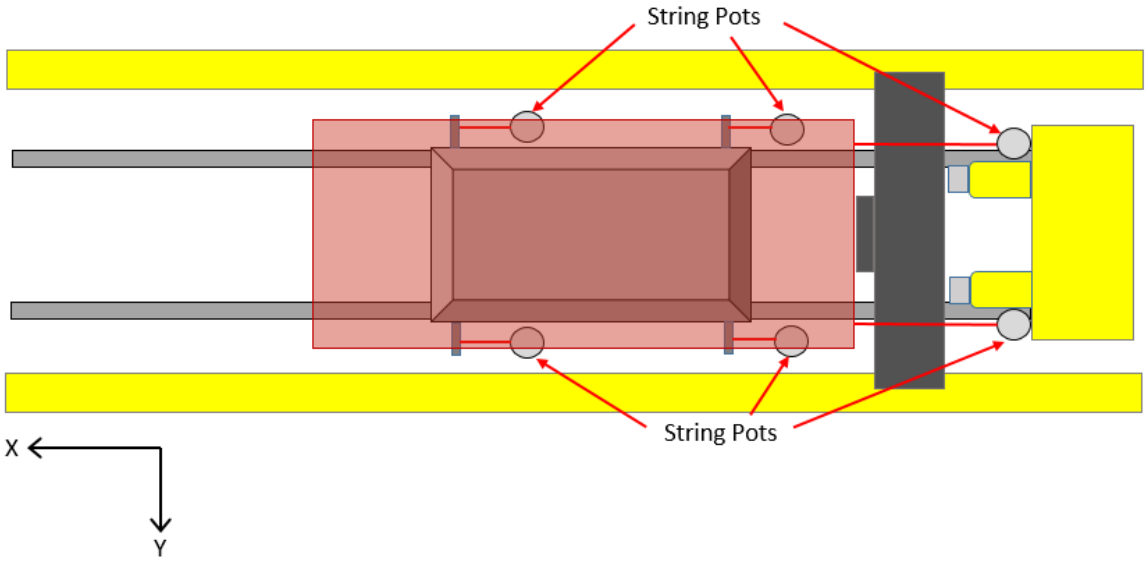

Figure 16. String Potentiometers (top view)

Table 2. String Potentiometers and Laser Sensor

Area	Location	Axis	Channel Name	Range
Fuel tank, lead end	Lead end, right corner	x	TDLRX	50 inches
Fuel tank, lead end	Lead end, left corner	x	TDLLX	50 inches
Fuel tank, trailing end	Trailing end, right corner	x	TDTRX	50 inches
Fuel tank, trailing end	Trailing end, left corner	x	TDTLX	50 inches
Boxcar, trailing end	Boxcar, right side	x	BDRX	50 inches
Boxcar, trailing end	Boxcar, left side	x	BDLX	50 inches
Fuel tank, middle	Mounting C-channel	z	LASERZ	N/A

2.6.4 Load Cells

Two load cells were used to measure forces being exerted on the fuel tank and the boxcar. One load cell was placed between the indenter and its longitudinal restraint to measure the force that the fuel tank exerted on the indenter. One load cell was placed at the trailing end of the boxcar between the boxcar end frame and the hydraulic cylinders to measure the force exerted on the boxcar by the hydraulic cylinders. Figure 17 and Figure 18 show the positioning of the load cells. Table 3 lists the locations for the load cells.

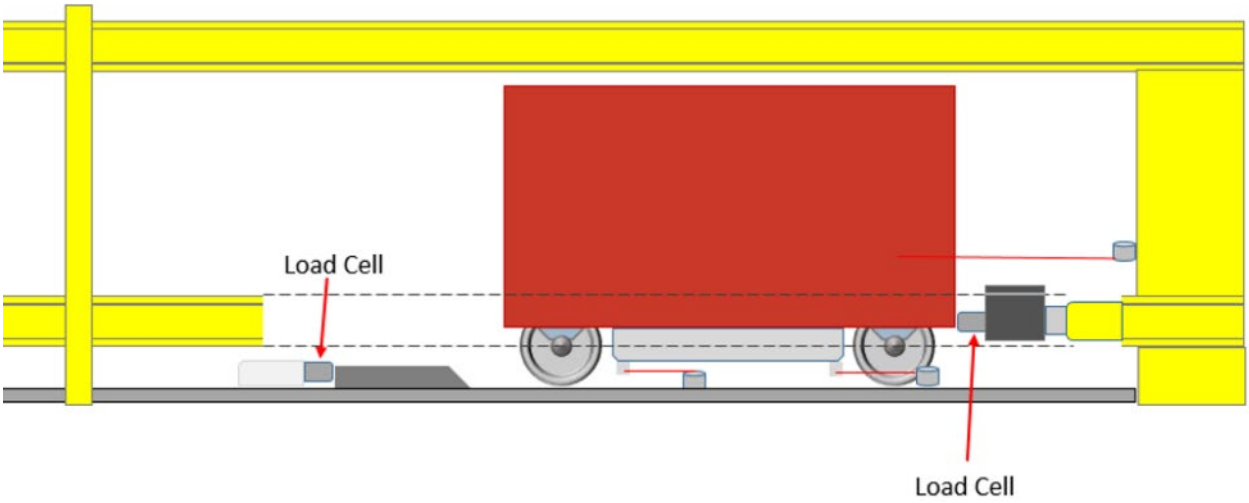

Figure 17. Load Cells (side view)

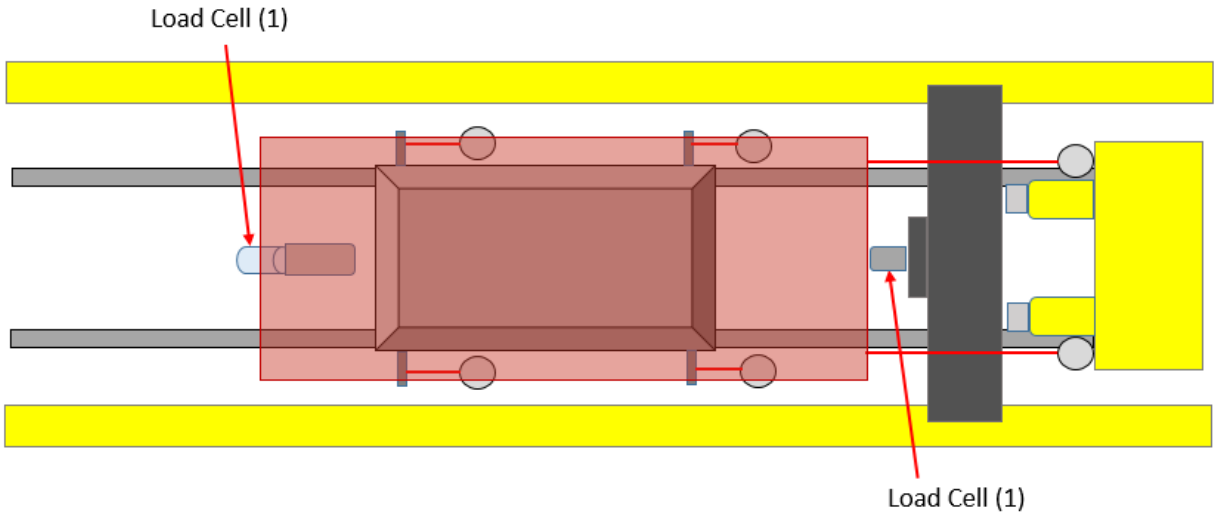

Figure 18. Load Cells (top view)

Table 3. Load Cells

Location	Axis	Channel Name
Indenter	x	IF
Boxcar trailing end	x	BF

2.6.5 Displacement, Pressure, and Force from Hydraulic Cylinders

The hydraulic cylinders output a reading of the stroke (displacement) and pressure. Table 4 shows the data channels from the hydraulic cylinders.

Table 4. Displacement, Pressure, and Force from Hydraulic Cylinders

Hydraulic Cylinder	Type of Data	Channel Name
Right	Displacement	HDR
Right	Pressure	HPR
Left	Displacement	HDL
Left	Pressure	HPL

2.6.6 Real-Time Photography

High-definition video cameras were used to document the raking impacts. Using one camera to stream video to an observer location, allowed the test to be monitored from a safe distance. This video was also recorded.

Final alignment and sighting of the cameras was done during the pre-test setup by positioning the boxcar in the squeeze fixture.

2.6.7 Data Acquisition

A set of data acquisition system recorded data from instrumentation mounted on the boxcar, fuel tank, and wayside. This system provided excitation to the instrumentation, analog-to-digital conversion, and recording of each data stream.

The data acquisition systems are Gantner Instruments Q.brixx A107 data acquisition units. Data from each channel was sampled and recorded at 25 Hz and filtered at 10Hz. Data recorded on the Q.brixx units was synchronized to time zero prior to the beginning of the test. Power to the Q.brixx units will be provided by 2.5 W, 10 to 30 VDC external power supplies.

2.6.8 Laser Scanning

The bottom surface of the fuel tank was scanned after testing. These scans allow for a direct comparison with pre- and post-test FE models by generating a digital, three-dimensional representation of the residual post-test deformation of the tank. These scans were done using a Trimble Total Station surveying device. The Trimble Total Station takes laser based distance measurements at discrete intervals. This results in a point cloud with variable density.

3. Analysis Overview

The research team performed pre-test modeling for each of the two raking tests on DMU fuel tanks. In general, using pre-test FE models assisted with the development of the test setup, estimating the expected loads and the overall response of the fuel tank to the raking scenario. The post-test model was refined based on the test results, and intended to aid in interpreting the results and examining the sequence of events that occurred during each test.

3.1 Raking Test 1 – December 2018

The performance of the pre-test FEA helped establish the desired indenter-to-fuel tank overlap, as well as to assist in developing the test setup itself. The Pre-test 1 model was assembled and meshed using the Abaqus/CAE software, and the simulation was executed using the Abaqus/Explicit software [10]. Prior to the first raking impact test, a previous modeling program had been used to develop a model of the DMU fuel tank to simulate a blunt impact test [2]. Researchers used this blunt impact DMU fuel tank model as the starting point for developing the raking impact model as the same fuel tank was being used in the first raking test as in the blunt impact test. After the first raking test, the pre-test FE model was updated to better reflect the test observations and measurements.

3.1.1 Pre-test 1 FE Model

The starting point for the first raking impact model was the post-test FE model from the blunt impact testing program [2]. The blunt impact FE model setup is shown in Figure 19 with the deformable DMU fuel tank annotated.

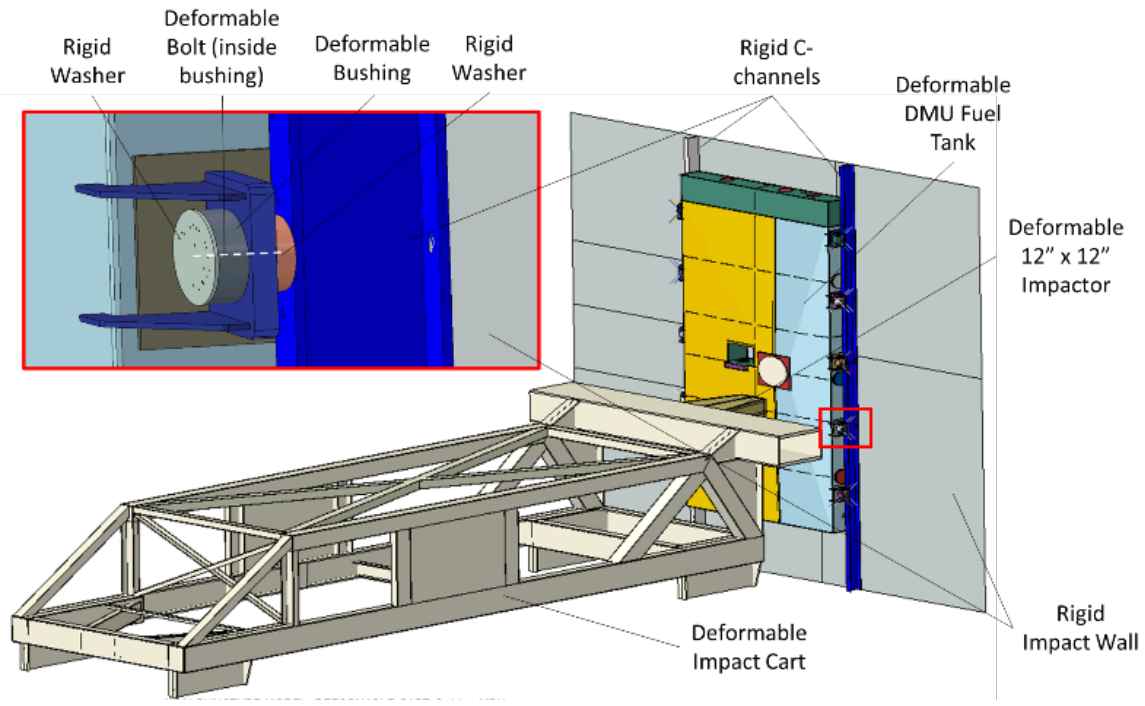

Figure 19. Blunt Impact FE Model Assembly with Annotations

The critical part of the blunt impact model to be transferred to the Pre-test 1 raking model was the DMU fuel tank itself. In the model built for the blunt impact testing program, the individual parts making up the DMU fuel tank were attached to one another using tied constraints. This methodology was maintained for the raking impact FE model.

Using the Pre-test 1 model for the first raking test assisted in developing the test setup as well as examining the response of the fuel tank to the raking scenario. In addition to the fuel tank, this model features many additional geometries, interactions, and constraints to examine how the overall test setup would perform. These additional mounting arrangement features include washers, bolts, bushings, and the C-channels to which the fuel tank was mounted. The mounting hardware was incorporated into the FE model to assist in the design of a mounting arrangement beneath the test boxcar that approximated the way the DMU fuel tank would be mounted beneath a DMU. Multi-Point Constraints (MPCs) were defined between the bolt hole in each mounting bracket and the top of each bolt. A second MPC was defined at the bottom of each bolt and the bottom surface of each deformable washer. Figure 20 shows an example mounting location from the Pre-test 1 raking model.

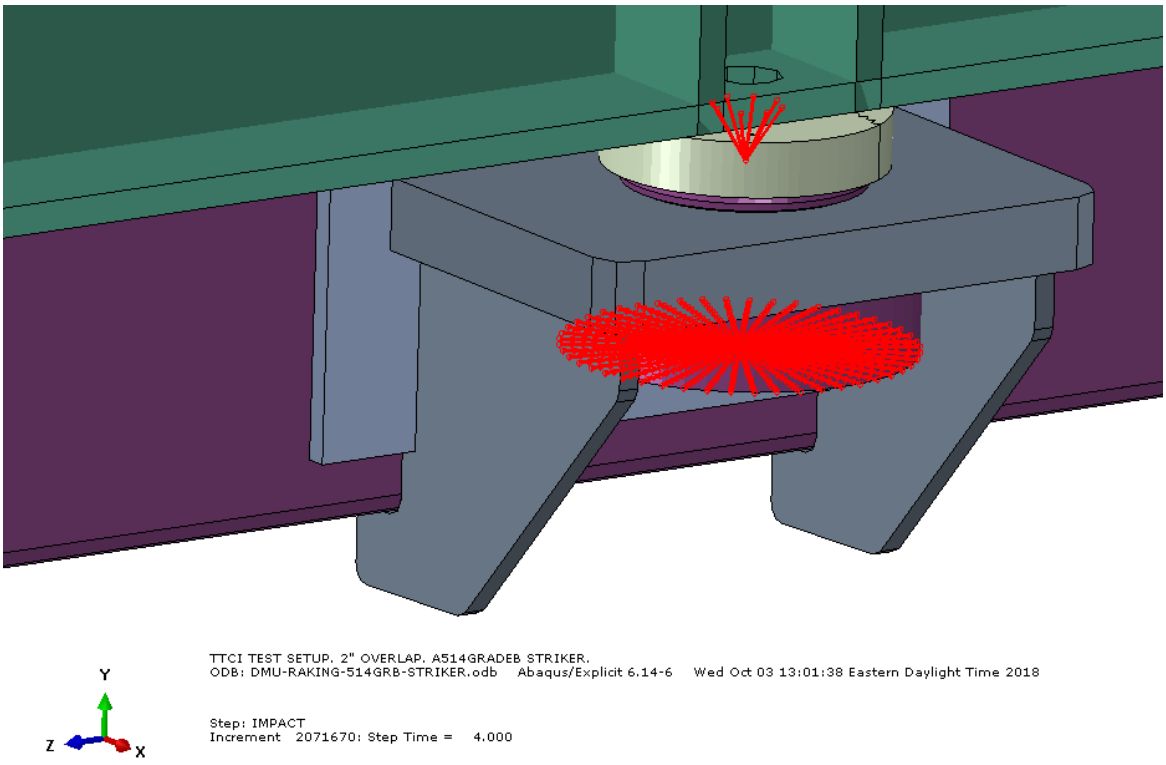

Figure 20. Typical Mounting Arrangement for Pre-test-1 Raking Model

In an ideal test setup, the applied load at the hydraulic actuators would be equal to the reaction load measured at the indenter, as this was a quasi-static test. However, there were several possible areas in the test setup where the load path could "short-circuit" and be transmitted to the ground without being measured by a load cell. Figure 21 is a schematic of the load path through the test setup.

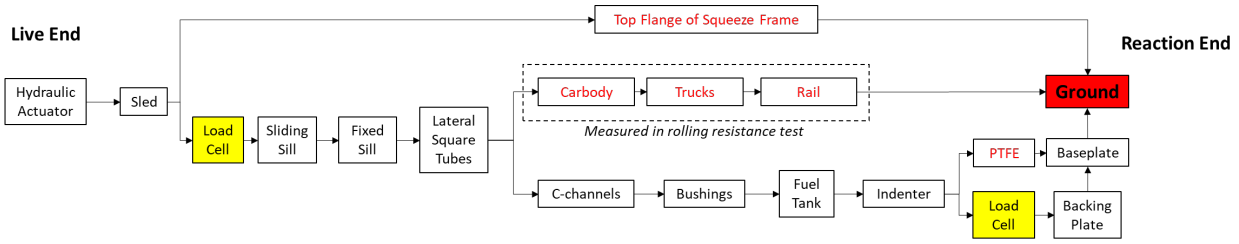

Figure 21. Schematic Flowchart of Load Path Expected in Test

Due to the locations in the load path where the load could be lost without being measured, a significant portion of the test setup beyond the DMU fuel tank had to be included in the model. Figure 22 presents an overall view of the Pre-test 1 FE model for raking test. This assembly includes parts representing several components in the load path, including the sills of the boxcar, the box beams, and the c-channels, as well as the bushings and mounting hardware between the fuel tank and c-channels. This assembly also included several parts representing fixed portions of the test setup including: the indenter, the baseplate, the PTFE shims between the bottom of the indenter and the baseplate, the backing plate connecting the load cell to the baseplate, and the load cell itself. Finally, the model included four rigid plates which served as fixed ends for springs attached to the corners of the fuel tank in the same manner as the string potentiometers in the physical test setup.

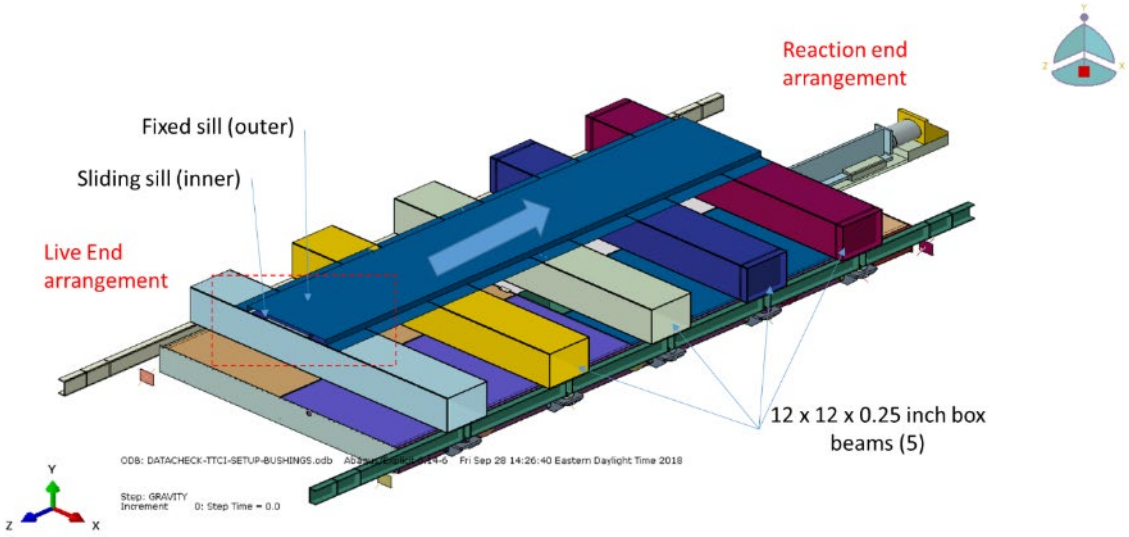

Figure 22. Overview of Pre-test 1 FE Model with Annotations

The Pre-test 1 model was run in two steps. First, a 1 G gravitational acceleration was applied to the model and the parts were allowed to settle over the course of 100 milliseconds (ms). The effects of gravity were thought to be important in this test because of the vertical loads imparted on the reaction end arrangement by the fuel tank as it contacts the indenter. If gravity were not included in the model, the DMU fuel tank would be pushed upward by the indenter more easily.

The second step was the impact step where the assembly representing the boxcar and the fuel tank move past the indenter. This step was 4 seconds in duration to allow a relatively slow displacement rate for the simulated boxcar.

Researchers used variable mass scaling with a target time increment of 4 $\times 10^{-6}$ seconds. This mass scaling increased the mass in the model by approximately 13 percent.

3.1.2 Geometry

Figure 23, the geometry of the fuel tank, illustrates the view from the top on the left, and the view from beneath the tank on the right. This geometry is the same as that used in the post-test blunt impact model, with a revised mesh. The tank used in the first raking test was deformed because it had been used in a previous blunt impact test. However, as the deformed area was at the opposite end of the tank from the end used in the first raking test, the Pre-test 1 FE model used geometry based on the undeformed shape of the fuel tank. During the test, this deformation required that only 8 of the 10 mounting locations be used to secure the fuel tank to the boxcar. As such, the Pre-test 1 FE model omitted mounting hardware at the same two locations.

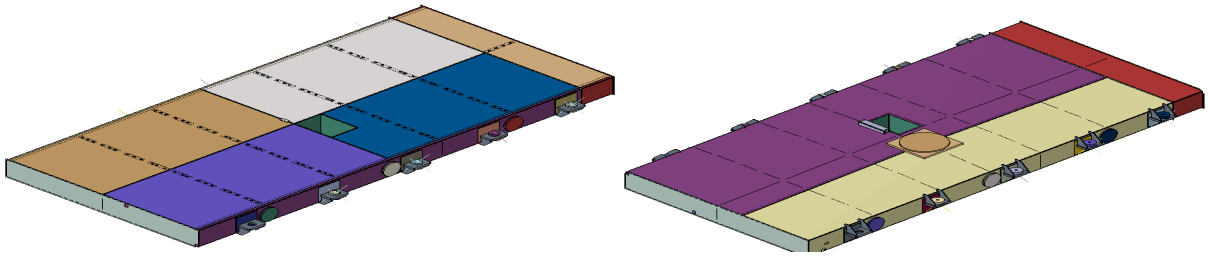

Figure 23. Fuel Tank in Pre-test-1 FE Model Viewed from Top (left) and Bottom (right)

The structure representing the boxcar and additional box beams and c-channels added to the boxcar to permit the fuel tank to be mounted (Figure 24). This image shows the view from above on the left and from underneath on the right.

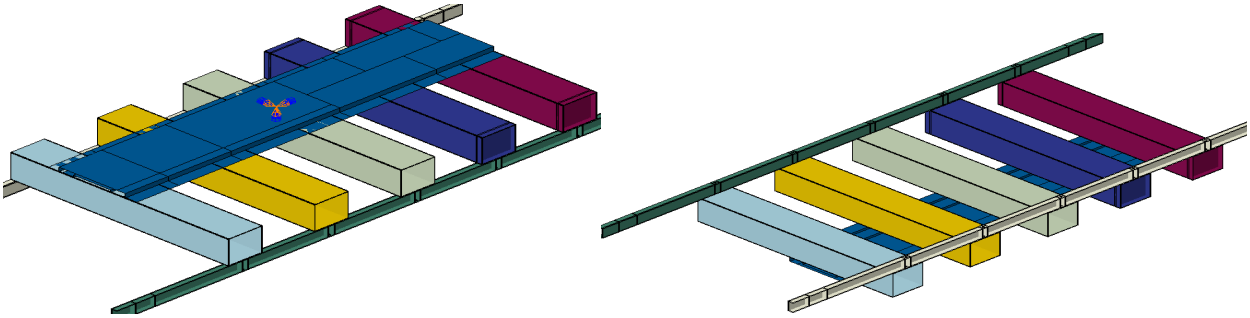

Figure 24. Boxcar and Mounting Structures in FE Model Viewed from Top (left) and Bottom (right)

The reaction end arrangement in the Pre-test 1 FE model included the baseplate, indenter, load cell, load cell backing plate, and PTFE shims. The reaction end arrangement is shown in Figure 25 with annotations indicating the different parts.

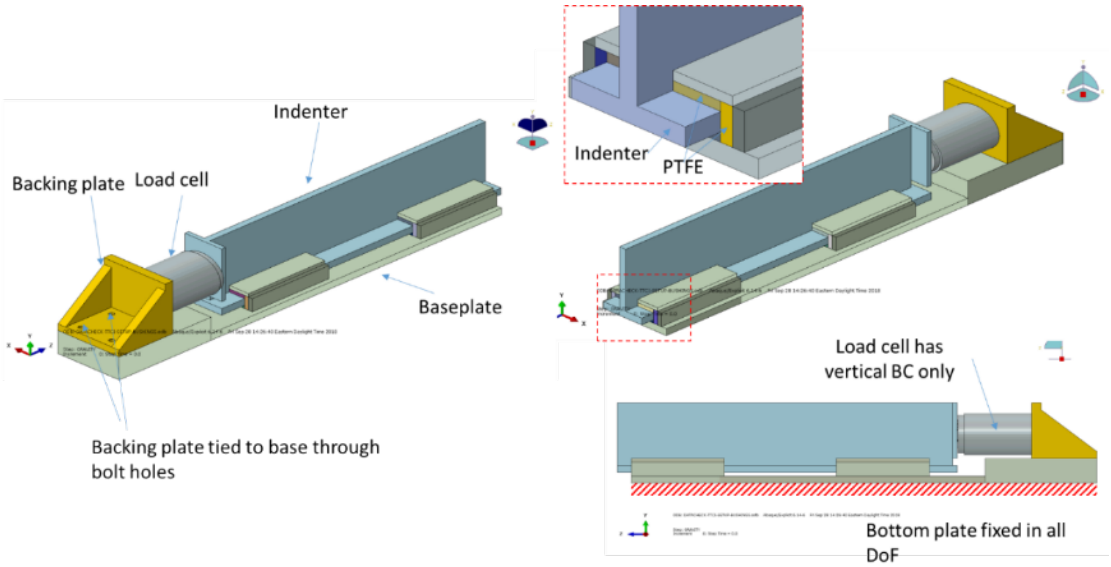

Figure 25. Reaction End Arrangement, Pre-test-1 FE Model

The initial positions of the reaction end assembly and the boxcar-tank assembly were adjusted so that, initially, the end plate of the fuel tank and the front face of the indenter were not in contact longitudinally and had an approximately 2-inch vertical overlap. The overlap is measured from the top edge of the indenter to the bottom edge of the fuel tank's end plate. Figure 26 illustrates the vertical overlap in the Pre-test 1 FE model.

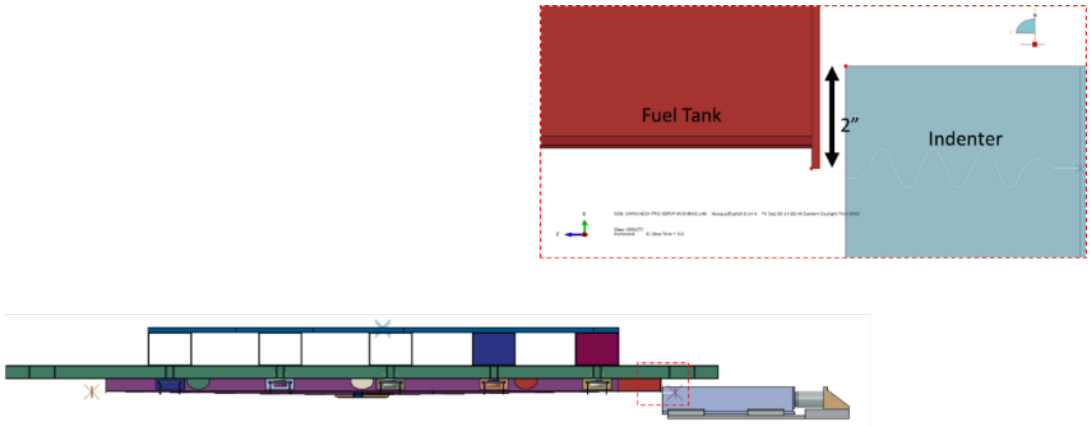

Figure 26. Side View of Pre-test-1 FE Model, Inset Showing Initial Vertical Overlap Between Indenter and Fuel Tank

While the DMU fuel tank itself was meshed using deformable shell elements, other structures within the assembly were meshed using other modeling techniques. Table 5 describes the mesh techniques used in the Pre-test 1 FE models.

Table 5. Summary of Mesh in Pre-test 1 FE Models

Part Name	Element Type	Number of Elements
Deformable backing plate	Reduced integration triangular shell (S3R)	34
	Reduced integration quadrilateral shell (S4R)	997
Deformable base plate	Reduced integration triangular shell (S3R)	22
	Reduced integration quadrilateral shell (S4R)	2,620
Deformable bolt	Quadratic beam (B32)	10
Deformable box beam	Reduced integration quadrilateral shell (S4R)	508*
Deformable bushing	Reduced integration hexahedral continuum (C3D8R)	8,400
Deformable C-channel	Reduced integration triangular shell (S3R)	154
	Reduced integration quadrilateral shell (S4R)	468
Deformable PTFE shims	Reduced integration hexahedral continuum (C3D8R)	1,040
Deformable indenter	Reduced integration hexahedral continuum (C3D8R)	4,372
Deformable DMU fuel tank	Reduced integration quadrilateral shell (S4R)	184,326
	Reduced integration triangular shell (S3R)	2,986
Rigid fixed sill	Rigid quadrilateral (R3D4)	588
	Mass element	1
	Rigid body reference node (RNODE3D)	12
Rigid sliding sill	Rigid quadrilateral (R3D4)	392
	Mass element	1
	Rigid body reference node (RNODE3D)	12
Rigid load cell	Mass element	1
	Rigid triangle (R3D3)	14
	Rigid quadrilateral (R3D4)	1,485
	Rigid body reference node (RNODE3D)	2
Rigid washer (thick)	Rigid quadrilateral (R3D4)	1,759
	Rigid triangle (R3D3)	36
	Mass element	1
	Rigid body reference node (RNODE3D)	1
Rigid plate	Rigid quadrilateral (R3D4)	4
	Rigid body reference node (RNODE3D)	1

*Element count for box beams with stiffening plates welded inside. For box beams without stiffening plates, 468 elements were used

3.1.3 Materials

Table 6 summarizes the materials defined in the DMU fuel tank in the Pre-test 1 FE model. The material definitions and properties in the Pre-test 1 FE model of the DMU fuel tank were based on the material definitions and properties used in the post-test model of the DMU fuel tank from

the blunt impact analysis Table 6. The material names below reflect the names used in the blunt impact testing report.

Table 6. Pre-test 1 Material Properties for DMU Fuel Tank FE Model

Region	Material
Bottom and sides	Side sheet steel (post-test)
Top	S235 steel (pre-test)
End sheets	End sheet steel (post-test)
Internal baffles	Baffle steel (post-test)

Table 7 defines the remaining deformable parts in the Pre-test 1 model, simplified elastic, elastic-plastic, or hyperelastic material properties.

Table 7. Pre-test Material Properties for Other Deformable Parts in FE Model

Part Name	Material
Deformable backing plate	36 ksi steel
Deformable base plate	36 ksi steel
Deformable bolt	Elastic steel
Deformable box beam	36 ksi steel
Deformable bushing	Rubber
Deformable C-channel	Elastic steel
Deformable PTFE shims	PTFE
Deformable indenter	A514 Grade B steel

Of the materials used in the model, only two new materials were introduced in the raking impact model that were not used in the previous blunt impact model. Those materials were the A514 Grade B steel used in the indenter, and the PTFE plastic used for the shims. Those material properties are described in this section.

A514 Grade B Steel

Table 8 lists the properties used for the ASTM A514 Grade B steel indenter in the FE. The models used a simple bi-linear stress-strain response for the material. Using this approach, the elastic portion of the stress-strain response is a line extending from the origin and having a slope equal to Young's Modulus. When the stress reaches the yield strength of the material, the plastic portion of the mechanical response follows a line with a decreased slope passing through the ultimate strength at a defined value of plastic equivalent strain.

Table 8. Mechanical Properties of ASTM A514 Grade B Steel used in FE Model

Property	Value	Units	Source
Modulus of Elasticity	200,000	MPa	–
Poisson's Ratio	0.3	–	–
Density	7.8×10^{-9}	Mg/mm^3	Matweb [11]
Yield strength	690	MPa	Matweb [11]
Ultimate strength	760	MPa	Matweb [11]
Plastic strain at ultimate	0.18	–	Matweb [11]

PTFE

Table 9 lists the properties used for the PTFE plastic shims placed between the baseplate and the indenter.

Table 9. Mechanical Properties of PTFE used in FE Model

Property	Value	Units	Source
Modulus of Elasticity	392	MPa	Piedmont Plastics [12]
Density	2.2×10^{-9}	Mg/mm^3	Piedmont Plastics [12]
Coefficient of friction (static, steel-on-PTFE)	0.2	–	Piedmont Plastics [12]

3.1.4 Boundary and Initial Conditions

A "Cartesian" type connector was used between the fixed sill and ground to estimate the rolling resistance of the boxcar. Additionally, a point mass was defined on the rigid fixed sill's reference point to represent the weight of the boxcar. A tabular force-versus-velocity relationship was defined for the connector element. At very low velocities, the connector element offered a high resistance force, approximating static friction. Once this initial high force is overcome, the resistance drops to a level that approximated the rolling resistance offered by the boxcar to further motion. This behavior was included in the pre-test model to investigate whether the boxcar would be likely to experience a sudden displacement as the load applied by the hydraulic actuators increased and the boxcar began to move.

Table 10 summarizes the connector behavior.

Table 10. Static and Rolling Resistance of Boxcar

Parameter	Value
Weight of boxcar (lbf)	87,300
Coefficient of static friction	0.3
Coefficient of rolling friction [13]	0.002
Static force of resistance (lbf)	26,200
Rolling force of resistance (lbf)	175

Table 11 lists the force versus velocity relationship for the Cartesian connector.

Table 11. Cartesian Connector Behavior

Velocity (in./s)	Force of Resistance (lbf)
-0.4	-175
-0.04	-175
-4×10^{-3}	-26,200
-4×10^{-3}	26,200
-0.04	175
-0.4	175

Figure 27 illustrates the boundary conditions and connectors defined in the Pre-test 1 raking model.

Figure 27. Pre-test 1 FE Model with Boundary Conditions

Table 12 summarizes the boundary conditions in the Pre-test 1 FE model, each step in the model, and defines a boundary condition of each region.

Table 12. Summary of Boundary Conditions in Pre-test 1 FE Model

Region	Step	Degrees of Freedom (DOF)	Value
Bottom of baseplate	All	1–3	Fixed
Rigid plates for string potentiometers	All	1–6	Fixed
Fixed sill	Gravity	1–6	Fixed
Fixed sill	Impact	1, 2, 4, 5, 6	Fixed
Sliding sill	Gravity	1–6	Fixed
Sliding sill	Impact	1, 2, 4, 5, 6	Fixed
Sliding sill	Impact	3	1,000 mm/s
Load cell	All	2	Fixed

3.1.5 Post-test 1 FE Model

The post-test FE model featured several changes based on the outcome of the first test. The post-test model was simplified to exclude those parts that did not significantly affect the test results.

Using variable mass scaling with a target time increment of 1×10^{-6} seconds, resulted in a 22 percent increase in mass in the model. A refined mesh was used and recalibrated material behaviors.

3.1.6 Geometry

The post-test FE model featured several changes based on the outcome of the first test. As many aspects of the test setup were found to perform as expected during the raking test, the post-test model was simplified to exclude those parts that did not contribute to the outcome of the test. The post-test model did not include the fixed or sliding sills of the boxcar, the box beams, or the c-channels as part of the mounting scheme. Additionally, removing the bushings and deformable bolts from the post-test model and replacing them with constraints simplified the load path into the tank's supports. The post-test FE model is shown in Figure 28 with its boundary conditions and constraints highlighted.

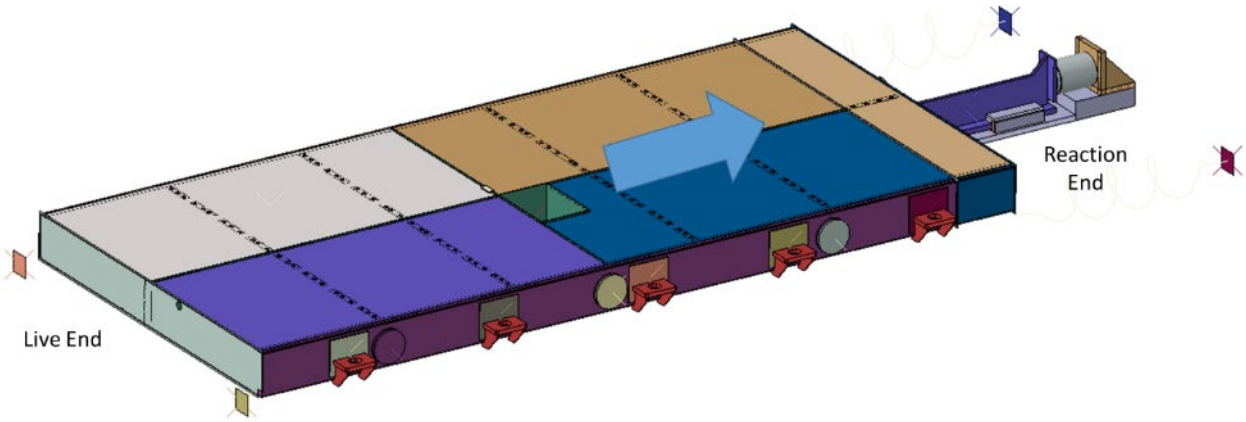

Figure 28. Overview of Post-test 1 FE Model

Several simplifications were also employed in this model to attempt to offset the increased runtime associated with the highly-refined mesh used in the Post-test 1 FE model. In the pre-test FE model, the indenter was meshed entirely with hexahedral "brick" elements. In the post-test model, only the tip of the indenter was meshed with "brick" elements, as the tip would be in contact with the bottom of the DMU fuel tank. The remainder of the indenter was meshed using shell elements to reduce the computational expense. Figure 29 shows the initial position of the indenter and the refined patch of elements. Note that this figure has been inverted, so that down in the image represents up in the test setup.

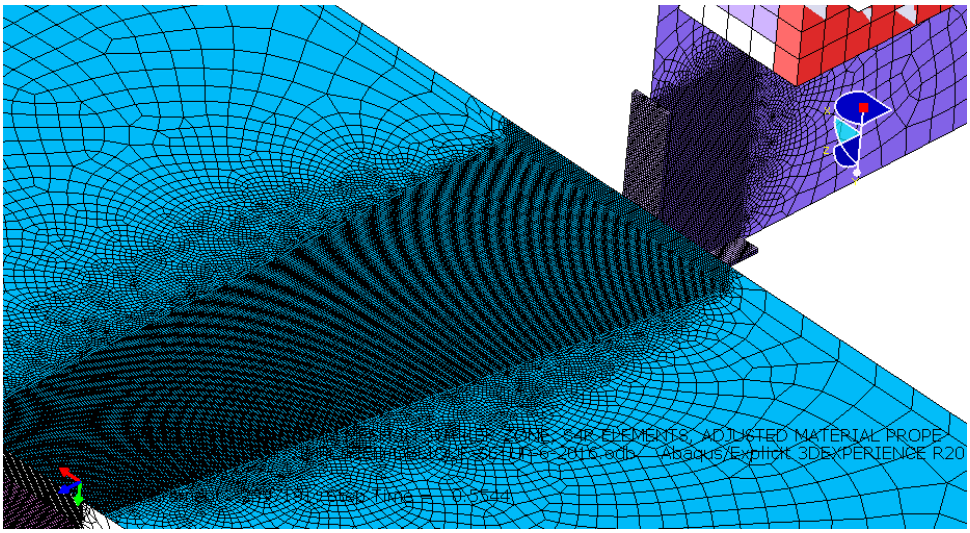

Figure 29. Refined Mesh on DMU Fuel Tank and Solid-shell Indenter, Post-test 1 FE Model

Areas of the fuel tank that were remote from the impact area, and thus expected to undergo only limited deformation during the test, were modeled as rigid bodies. Figure 30 shows the areas of the DMU fuel tank that were modeled as rigid bodies in the Post-test 1 FE model. The multi-colored areas are modeled as deformable bodies, while the white areas are rigid bodies. The top of Figure 30 shows the Post-test 1 FE model viewed from above, while the bottom illustration shows the model when viewed from below.

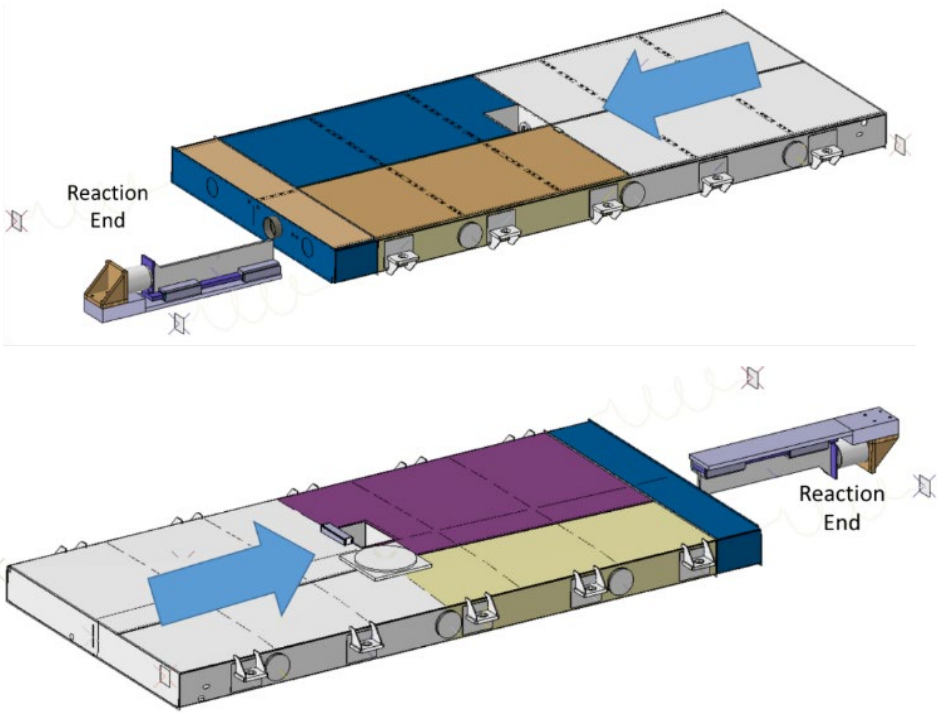

Figure 30. Deformable and Rigid Sections of DMU Fuel Tank in Post-test 1 FE Model Viewed from Above and Below

The Post-test 1 DMU fuel tank was meshed using a combination of deformable and rigid shell elements to reduce the model's runtime. The indenter was not observed to have any significant permanent deformation following the test, so the Post-test 1 FE model used a rigid indenter.

Table 13 summarizes the mesh techniques used in the Post-test 1 FE model.

Table 13. Summary of Mesh in Post-test-1 FE Models

Part Name	Element Type	Number of Elements
Deformable backing plate	Reduced integration triangular shell (S3R)	34
	Reduced integration quadrilateral shell (S4R)	997
Deformable base plate	Reduced integration triangular shell (S3R)	22
	Reduced integration quadrilateral shell (S4R)	2,620
Deformable PTFE shims	Reduced integration hexahedral continuum (C3D8R)	1,040
Indenter	Reduced integration hexahedral continuum (C3D8R)	4,372
DMU fuel tank	Reduced integration quadrilateral shell (S4R)	265,535
	Reduced integration triangular shell (S3R)	5,858
	Rigid triangle (R3D3)	154
	Rigid quadrilateral (R3D4)	36,939
Rigid plate	Rigid quadrilateral (R3D4)4	4
	Rigid body reference node (RNODE3D)	1

The Post-test 1 model was run in one step. Because of the simplified support structure at the bolt holes, a 1 G gravity settling step was not used in this model because the bushings and beams representing the carbody mounting structure had been removed. In the run step, the fuel tank moved past the indenter. This step was 4 seconds in duration to allow a relatively slow displacement rate for the simulated boxcar.

3.1.7 Materials

Based on the pre-test model overestimating the forces necessary to cause tearing and the observation that the tearing in the test was highly-localized to the area around the indenter, a highly-refined mesh was used in the Post-test 1 FE model. This highly-refined mesh (Figure 29) was used on the bottom and end sheets on the Post-test 1 DMU fuel tank model. The area of refined mesh.

The damage initiation envelope for the end plate was re-calibrated for use with the finer mesh in the post-test FEA. The pre-test damage initiation envelopes were maintained for the steel materials used for the bottom sheet and the baffles. Figure 31 shows the Pre- and Post-test 1 damage initiation envelopes for the end sheet steel.

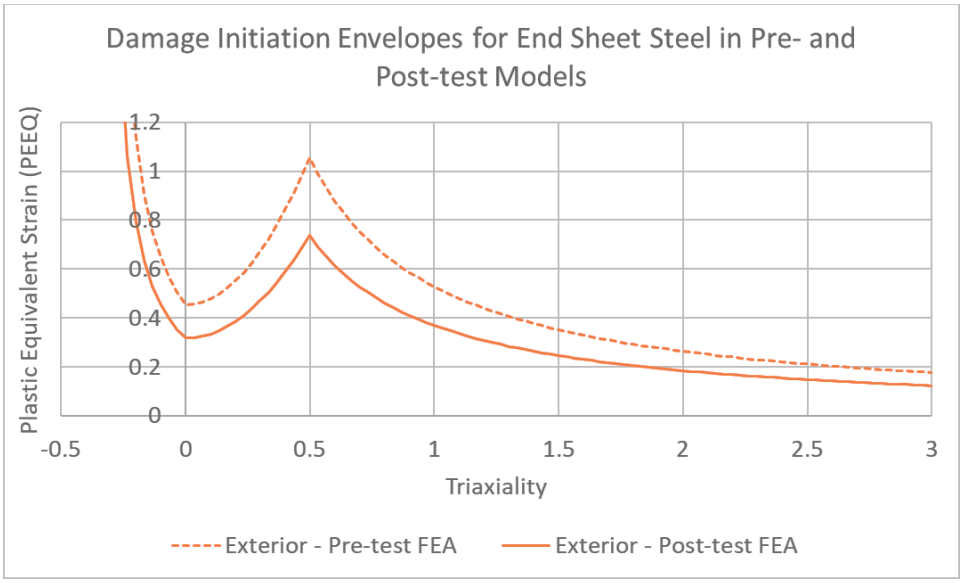

Figure 31. Damage Initiation Envelopes for End Sheet Steel in Pre- and Post-test Models

The damage progression values for the material models used on the bottom sheet of the tank and the endplate needed to be recalibrated for the smaller elements in the refined mesh. The damage progression value for the pre-test baffle steel was not changed in the Post-test 1 model. Table 14 summarizes the progression values.

Table 14. Pre- and Post-test Damage Progression Values from Raking Test 1 FE Models

	Value in Pre-test Model	Value in Post-test Model
Side sheet steel	3,000	280
End sheet steel	3,000	280
Baffle steel	5,000	5,000

3.1.8 Boundary and Initial Conditions

The Post-test 1 FE model used rigid brackets along the edges of the tank. The bushings, washers, and bolts from the pre-test model were not used in the post-test model, since they did not appear to contribute to the results of the test. Each bracket was given a prescribed 610-mm (24-inch) displacement that ramped up over the course of 0.82 seconds, simulating the fuel tank's progress across the indenter. The bolt holes were also prevented from moving in the remaining five DOF. Table 15 summarizes the boundary conditions used in the Post-test 1 FE model.

Table 15. Summary of Boundary Conditions in Post-test-1 FE Model

Region	Step	DOF	Value
Bottom of baseplate	All	1–3	Fixed
Rigid plates for string potentiometers	All	1–6	Fixed
Rigid brackets	All	1, 2, 4, 5, 6	Fixed
Rigid brackets	All	3	610 mm

Region	Step	DOF	Value
Baseplate	All	1-3	Fixed
Load cell	All	2	Fixed

3.2 Raking Test 2 – November 2019

The starting point for Pre-test 2 model was the Post-test 1 model. The Pre-test 2 model continued the approach of using a refined mesh, a simplified representation of the mounting hardware, and a combination of rigid and deformable areas on the fuel tank to reduce simulation runtime.

3.2.1 Pre-test 2 FE Model

The Pre-test 2 model was used to examine several different lateral positions of the indenter. These positions were intended to explore whether the tank is more vulnerable to tearing from a raking impact to different areas of the bottom of the tank. Test 2 targeted the same end of the DMU fuel tank as had been raked in the first test. Three potential locations were examined using the Pre-test 2 model:

- Indenter shifted laterally in the +X direction, adjacent to the tank's longitudinal baffle.
- Indenter shifted laterally in the +X direction, halfway between the longitudinal baffle and Test 1 position.
- Indenter shifted laterally un the –X direction, halfway between tank's edge and longitudinal weld seam position.

Figure 32 shows the three lateral positions of the indenter.

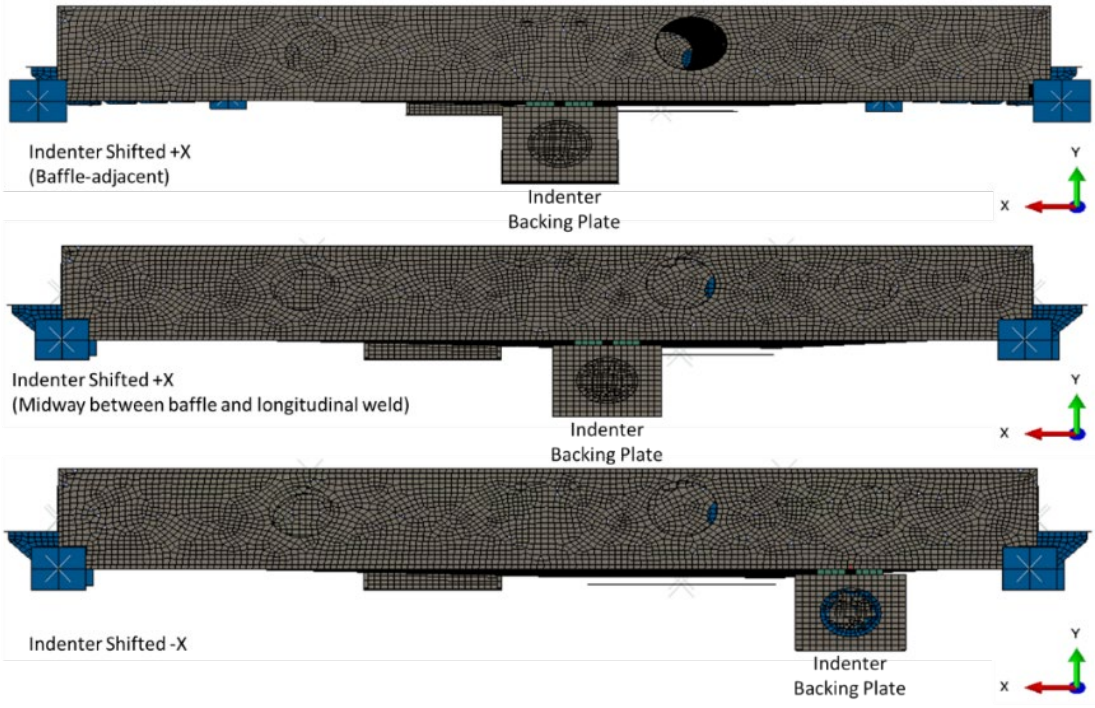

Figure 32. Three Lateral Positions of Indenter Examined in Pre-test 2 Model

For any of the three locations chosen, the vertical overlap between the top of the indenter and the bottom of the fuel tank would increase as the displacement of the fuel tank increased due to the tank's sloped bottom sheet. The indenter's height under the tank was limited to prevent it from contacting the end sheet of the tank, which extended lower than the tank's bottom sheet.

Based on the desired outcome of a tearing the tank, the limitations of the clearances and the overall test setup, and the anticipated forces involved, the indenter was positioned midway between the baffle and the longitudinal weld for raking Test 2.

Variable mass scaling with a target time increment of 2×10^{-6} seconds was used, resulting in an additional mass of 153 percent. As the loading was intended to be quasi-static, this additional mass was not anticipated to have a significant effect on the overall fuel tank response to the raking impact.

3.2.2 Geometry

The geometry of the DMU fuel tank used in the Pre-test 2 FE model is based on the geometry used in the Post-test 1 FE model. The most significant change to the geometry is the area of refined mesh in the Pre-test 2 model. Since the position of the Indenter has been shifted laterally, the refined patch of elements in the DMU fuel tank has also been shifted laterally to place it in the path of the indenter. The geometry of the Pre-test 2 FE model is shown in Figure 33, with the boundary conditions indicated. Note that the top of this figure shows the model viewed from underneath, and the bottom of this figure shows the model viewed from above.

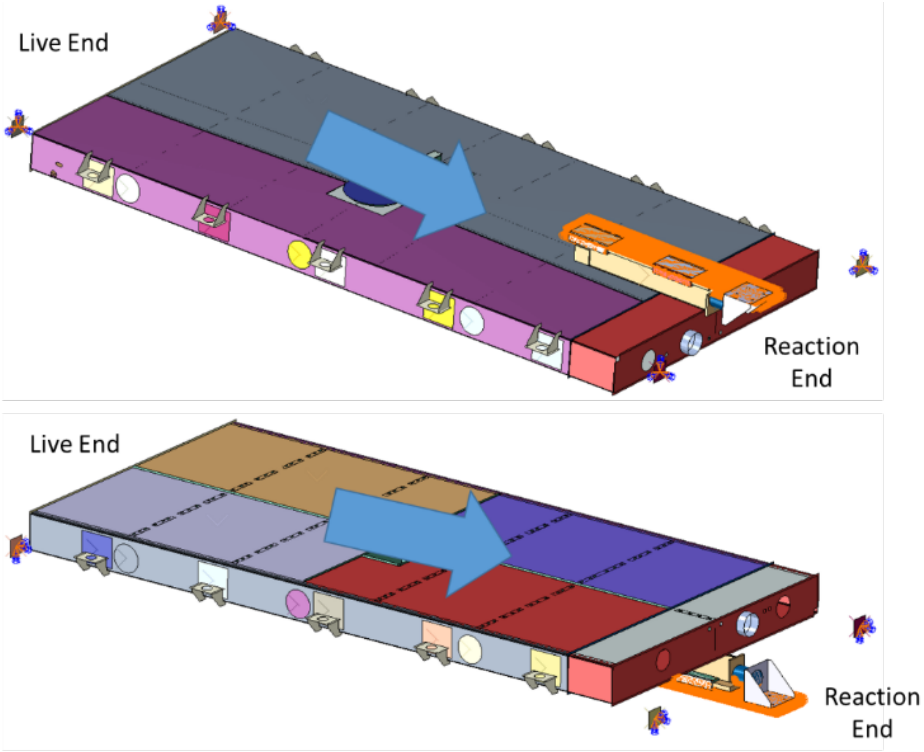

Figure 33. Pre-test-2 FE model Setup, Indenter Shifted between Test 1 Position and Longitudinal Baffle

Similar to the Post-test 1 FE model, the Pre-test 2 FE model used a refined mesh of elements (approximately 1 mm, or 0.04 inch) in the path of the indenter. Figure 34 depicts this zone of refined elements.

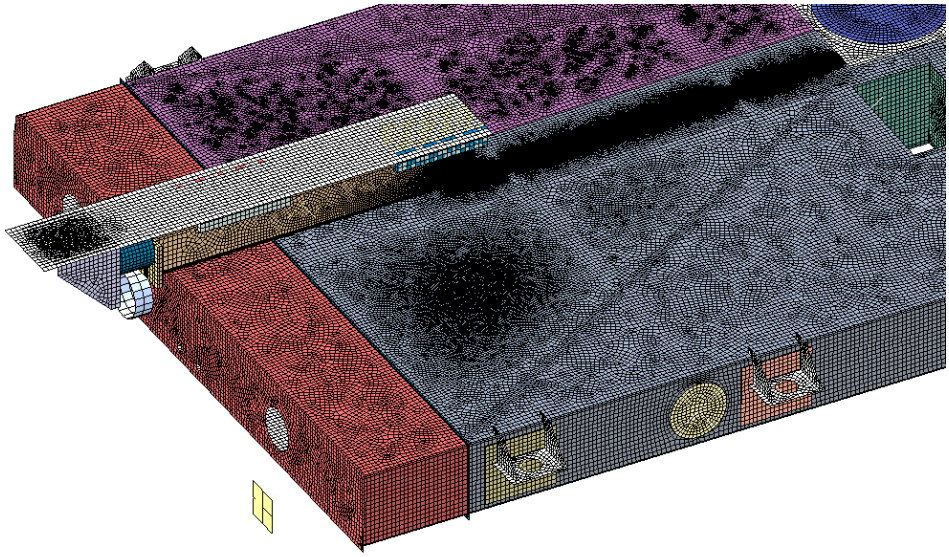

Figure 34. Refined Mesh in Path of Indenter, Pre-test-2 FE Model

The indenter geometry has been modified in the Pre-test 2 model to match the indenter modifications used in Test 2. The indenter height was reduced between first and second raking tests to prevent the indenter from contacting the endplate. This allowed the indenter's initial position to be further under the DMU fuel tank and reduced the likelihood that the tank's end plate would contact the back of the indenter. The indenter was initially positioned with its tip in contact with the fuel tank's bottom sheet, to maximize the available stroke of the hydraulic actuators. In the FE model, the clearance between the top of the indenter and the bottom of the end plate was chosen to be 1 mm (0.04 inch). Figure 35 shows the initial position of the indenter in the Pre-test 2 FE model.

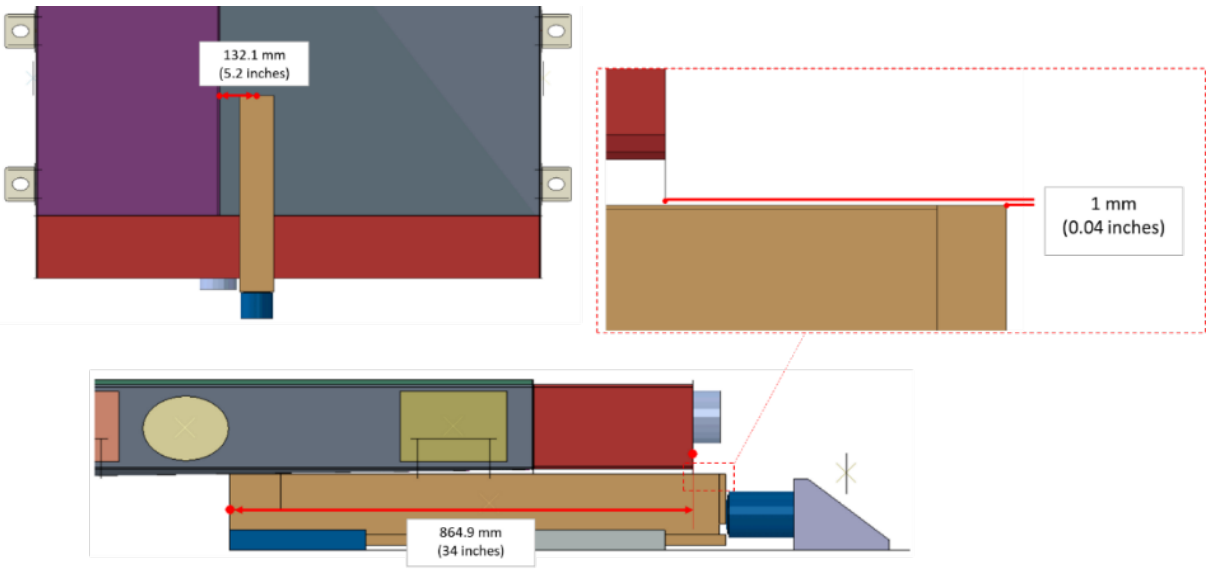

Figure 35. Initial Position of Indenter Relative to DMU Fuel Tank, Pre-test-2 Model

The Pre-test 2 model featured areas of the DMU fuel tank and other parts that were modeled as rigid bodies, similar to the Post-test 1 model. Areas of the fuel tank that were remote from the impact area and thus, expected to undergo limited deformation during the test, were modeled as rigid bodies. Figure 36 shows the areas of the DMU fuel tank that were modeled as rigid bodies in the Pre-test 2 FE model. The multi-colored areas are modeled as deformable bodies, while the white areas are rigid bodies. The top of Figure 36 shows the Pre-test 2 FE model viewed from above, while the bottom of this figure shows the model when viewed from below.

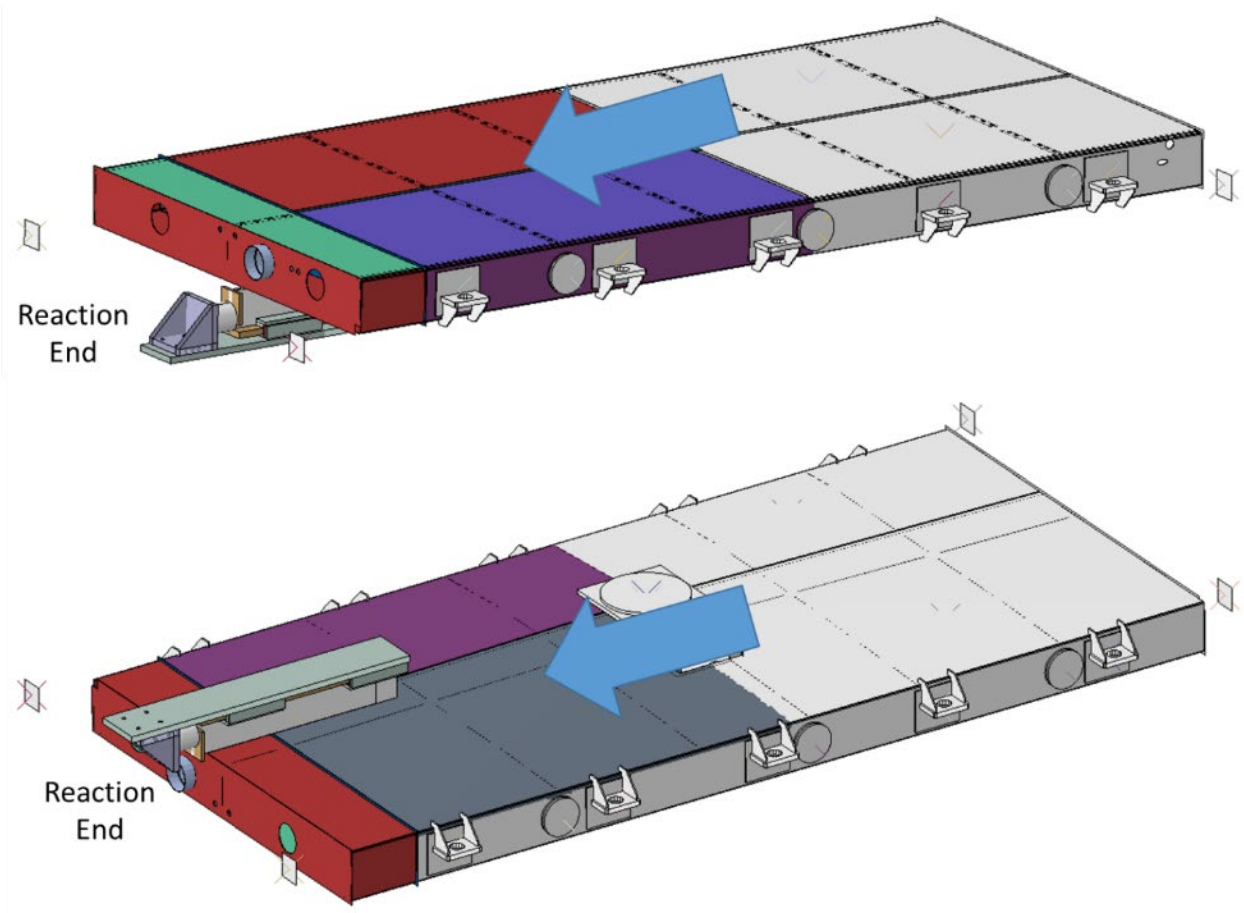

Figure 36. Deformable and Rigid Sections of DMU Fuel Tank in Pre-test-2 FE Model Viewed from Above and Below

The Pre-test 2 DMU fuel tank was meshed using a combination of deformable and rigid shell elements to reduce the model's runtime. The indenter was not observed to have any significant permanent deformation following the test, so the Post-test 1 FE model used a rigid indenter. Table 16 summarizes the mesh techniques used in the Post-test 1 FE model.

Table 16. Summary of Mesh in Pre-test-2 FE Models

Part Name	Element Type	Number of Elements
Deformable backing plate	Reduced integration triangular shell (S3R)	34
	Reduced integration quadrilateral shell (S4R)	957

Part Name	Element Type	Number of Elements
Deformable base plate	Reduced integration triangular shell (S3R)	30
	Reduced integration quadrilateral shell (S4R)	2,693
Deformable PTFE shims	Reduced integration hexahedral continuum (C3D8R)	200
Indenter	Reduced integration hexahedral continuum (C3D8R)	178,228
	Reduced integration quadrilateral shell (S4R)	3,999
DMU fuel tank	Reduced integration quadrilateral shell (S4R)	235,206
	Reduced integration triangular shell (S3R)	6,263
	Rigid triangle (R3D3)	154
	Rigid quadrilateral (R3D4)	36,939
Rigid plate	Rigid quadrilateral (R3D4)	4
	Rigid body reference node (RNODE3D)	1

The Pre-test 2 model ran in two steps. The first impact step ran for 500 ms and ran to completion. A continuation step ran for a further 250 ms of impactor travel.

3.2.3 Materials

The Pre-test 2 FE model used the same material behaviors as the Post-test 1 FE model.

3.2.4 Boundary and Initial Conditions

The boundary conditions applied to the Pre-test 2 FE model were similar to the boundary conditions used in the post-test 1 FE model. One difference was the boundary condition applied to the DMU fuel tank to move it across the indenter. Where the Post-test 1 FE model used a displacement boundary condition that ramped up over a prescribed time, the Pre-test 2 FE model used a constant velocity boundary condition of 1,000 mm/second (39.4 inches/second). Table 17 summarizes the boundary conditions in the Pre-test 2 FE model.

Table 17. Summary of Boundary Conditions in Pre-test 2 FE Model

Region	Step	DOF	Value
Bottom of baseplate	All	1–3	Fixed
Rigid plates for string potentiometers	All	1–6	Fixed
Rigid brackets	All	1, 2, 4, 5, 6	Fixed
Rigid brackets	All	3	1,000 mm/sec
Baseplate	All	1–3	Fixed
Load cell	All	2	Fixed

4. Results – Tests and Analyses

This section first presents the results from each of the two raking tests including test measurements, mode of deformation, and any key observations on the test setup or the response of the fuel tank to the raking scenario. This section then presents a comparison between the FE modeling of each test and the corresponding test results.

4.1 Raking Test 1 Results

Researchers conducted the first raking test on December 18, 2018, at the TTC. The boxcar was positioned in the squeeze fixture with the leading end plate against the edge of the indenter. The indenter was positioned with 2 inches of overlap between the top of the indenter and the bottom of the tank's end plate, as shown in Figure 11. During the test, the indenter punctured into the end plate of the tank and tore through the bottom sheet of the tank. The indenter was pushed at a rate of 1.2 inches per minute for a length of 22.6 inches. Tearing in the fuel tank was initiated at the tank's end sheet and progressed for the full 22.6 inches of travel. Deformation in the fuel tank was localized to the area near the tear. The internal baffles deformed as the indenter passed through the cross section of the tank where the baffles are located. There was no visible deformation in the fuel tank mountings. Figure 38 shows the tear in the fuel tank's bottom sheet.

Figure 37 and Figure 38 provide post-test photographs of the torn area on the edge and bottom surface of the DMU fuel tank. As the indenter made initial contact, the end plate material was pushed back and the bottom sheet was pushed down. As the applied force increased, the end plate began to tear. Once the end plate tore, the fuel tank could continue raking over the indenter with contact mainly between the bottom sheet of the tank and the indenter. The path of the indenter is visible in Figure 38, where the tear in the bottom sheet is clean and approximately the width of the indenter. The position of the first set of internal lateral baffles can be seen where the bottom sheet separated from the baffles in the area near the tear, creating a roughly triangular hole. When the indenter reached this internal baffle, the baffle material was deformed backward until it was fully penetrated, allowing the indenter to continue tearing the fuel tank's bottom sheet.

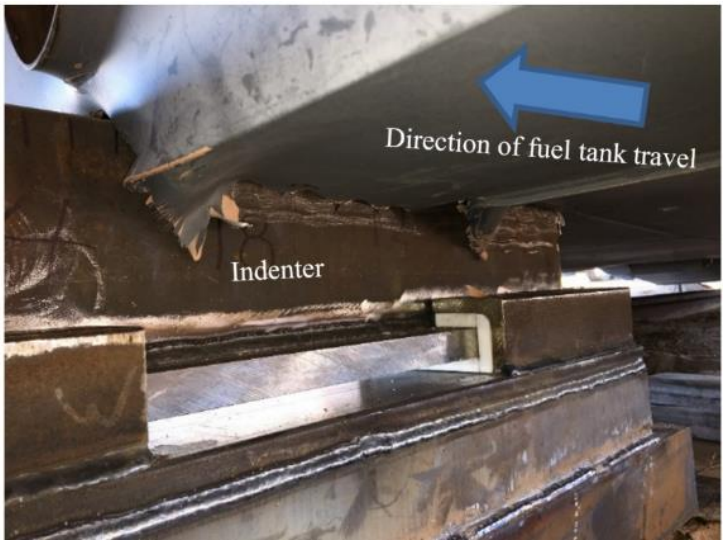

Figure 37. Post-test Photograph of Indenter and Tank

Figure 38. Tear in Test 1 Fuel Tank

4.1.1 Test 1 Measurements

Figure 39 shows the measured forces of the two load cells versus time. These were measured at the point of load application at the end of the boxcar, and at the point of load reaction at the indenter. The load cell placed between the hydraulic cylinder/sled assembly and the boxcar is labeled "BF" ("boxcar force") and the load cell between the indenter and base plate is labeled "IF" ("indenter force"). The load application load cell was about 30 feet away from the reaction load cell. The plot shows force over the full duration of the test. The plot shows very good agreement between these two load cells, indicating that there was no significant force lost due to the test setup.

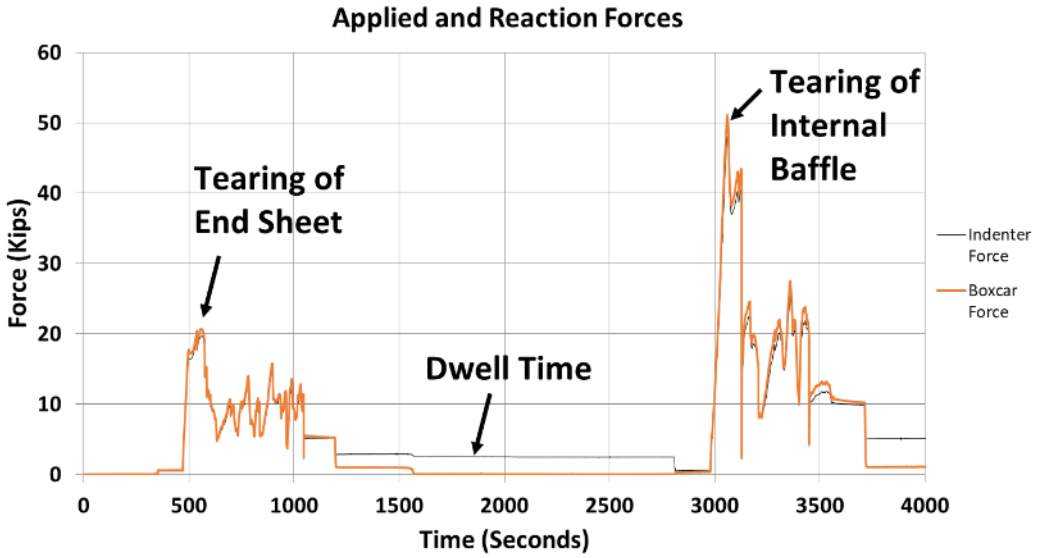

Figure 39. Comparison of Applied and Reaction Forces

The indenter contacted the edge of the fuel tank and as the force began to climb to an initial peak load of about 20,000 lbf at 500 seconds the end sheet tears. The force then dropped to an average load of around 10,000 lbf as the indenter pushed through the bottom sheet of the tank. The hydraulic actuator used in this test had a stroke of 11 inches. The "dwell time" shown on the Figure 39 plot marks the period when the hydraulic actuator had to be reset to allow for a second push up to 21 total inches of raking. At about 3,000 seconds, the test resumed and the force climbed to a second peak load of around 51,000 lbf as the indenter reached an internal baffle. The indenter tore through the baffle and the force dropped off significantly for the remaining stroke of the hydraulic cylinders. The test was terminated at 21 inches of displacement.

Figure 40 shows the force-versus-displacement measurements. The force measurements from the load cells are plotted against the string potentiometer data. As shown, force measurements at the application load cell and the reaction load cell did not deviate more than approximately 3,000 lbf from each other. The maximum force measured during this test was approximately 51,000 lbf and was measured at a raking distance of 12.6 inches.

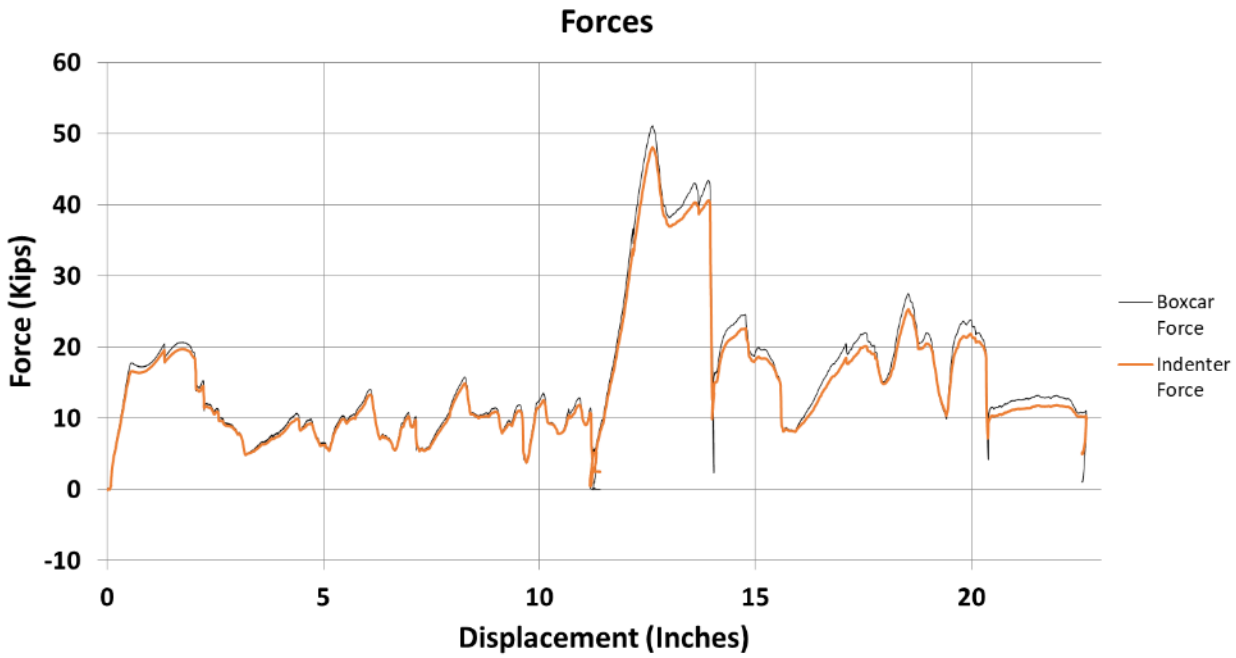

Figure 40. Test 1 Combined Force vs. Displacement Measurements

A laser displacement transducer was positioned to measure the vertical displacement of one of the c-channels to which the fuel tank was mounted. As the displacement history in Figure 41 shows, the vertical movement was negligible.

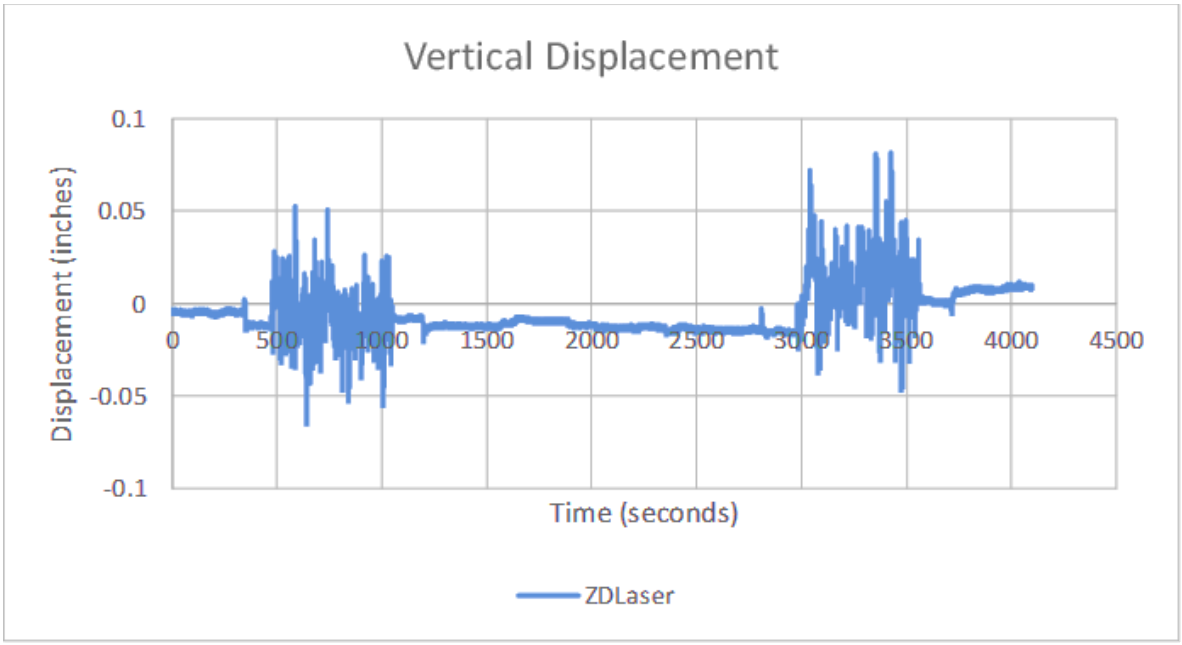

Figure 41. Laser Scan Measurement of Vertical Displacement

Displacements of the boxcar and the fuel tank relative to the ground were measured with string potentiometers. Figure 42 shows that the four string potentiometers mounted on the four corners of the fuel tank measured a consistent longitudinal displacement with left and right sides of the boxcar. Each measurement shows two distinct periods of 11 inches of increasing displacement with the stationary dwell time in-between.

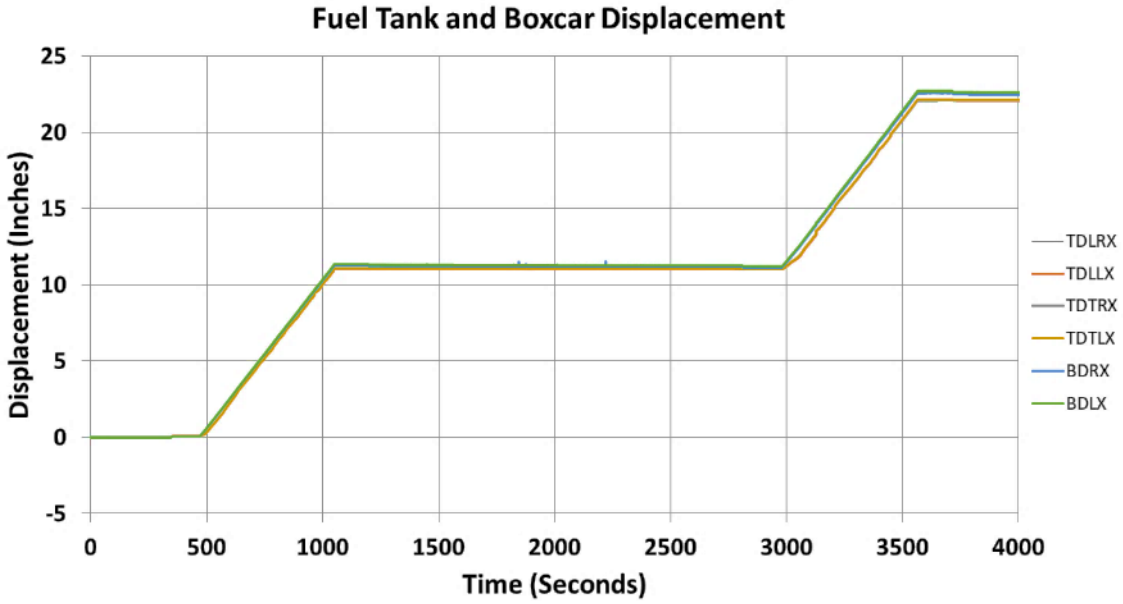

Figure 42. Test 1 Combined Displacement Measurements

After test completion, a laser scan was performed on the fuel tank in the area near the tear. Scan data revealed that the deformation of the tank's bottom sheet appeared to be minimal in areas not

close to the tear. The point cloud also shows the basic shape of the tear in the tank's bottom sheet. Figure 43 provides an image of the point cloud.

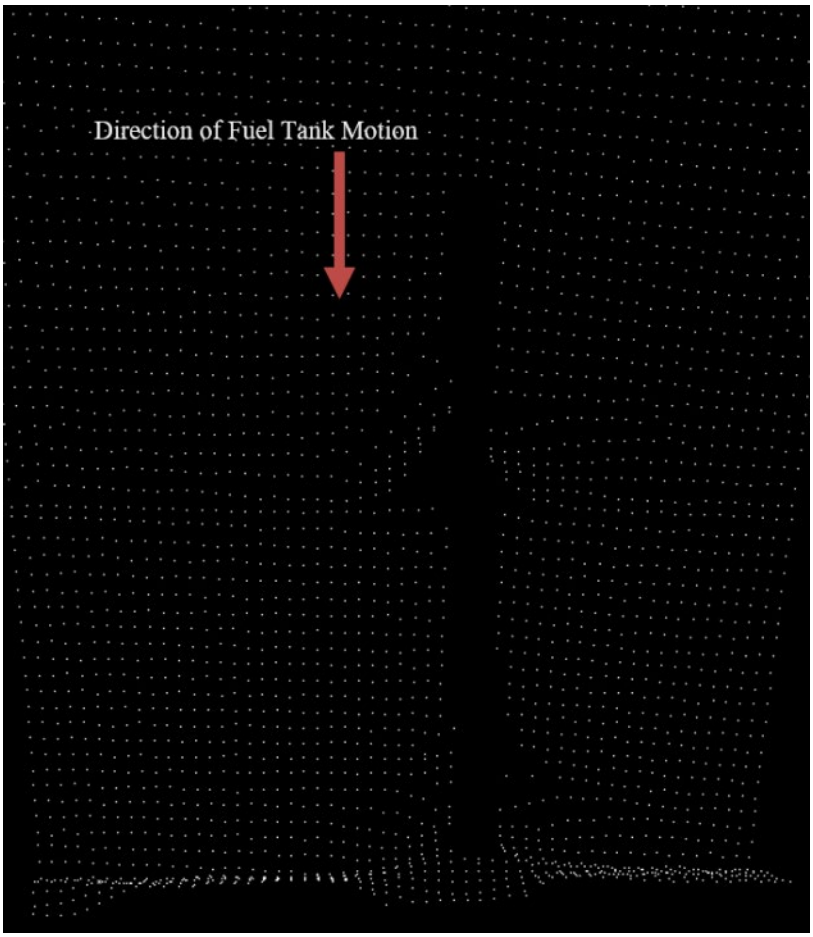

Figure 43. Test 1 Scan Point Cloud – Bottom View

4.2 Raking Test 2 Results

During this test, the boxcar was pushed for a distance of 44.2 inches. Tearing in the fuel tank occurred at the first internal, longitudinal baffle and proceeded for approximately 1 inch. However, this tear was localized to the area near the baffle. The indenter continued to scrape the surface of the fuel tank, without tearing, for approximately 22 inches. Tearing in the fuel tank was reinitiated near the second internal, longitudinal baffle. As in the first test, deformation in the fuel tank was localized to the area near the tear. No significant deformation was observed in the fuel tank mountings. The tears in the fuel tank's bottom sheet are shown in Figure 44 through Figure 46.

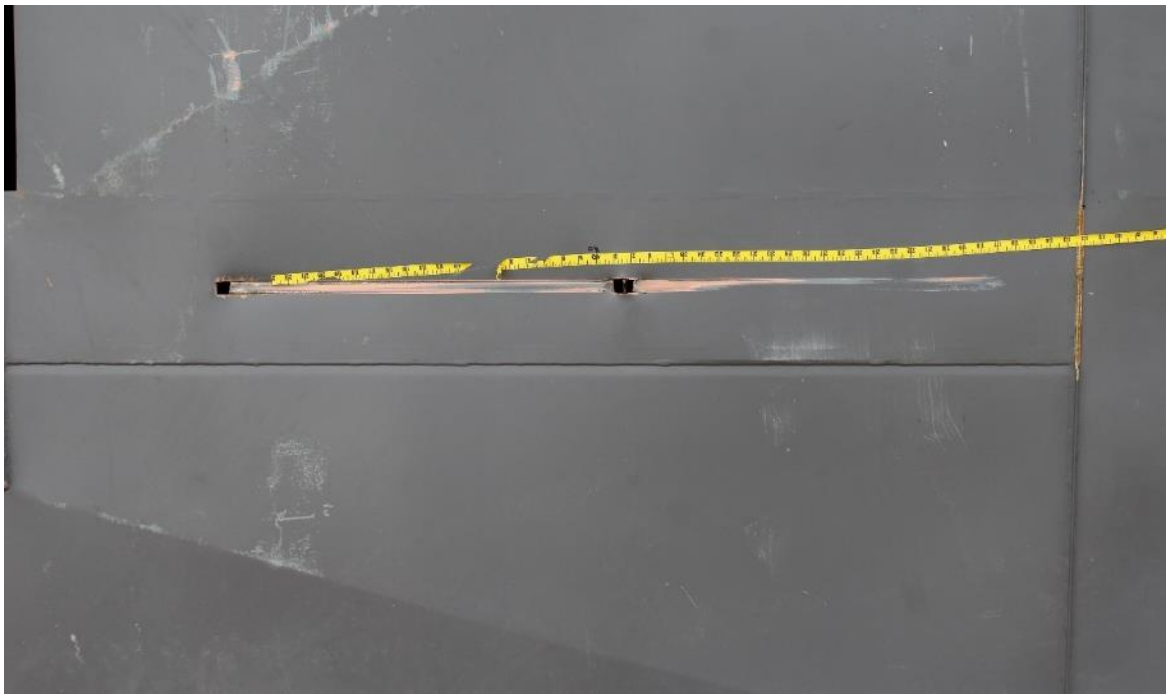

Figure 44. Tears in Test 2 Fuel Tank

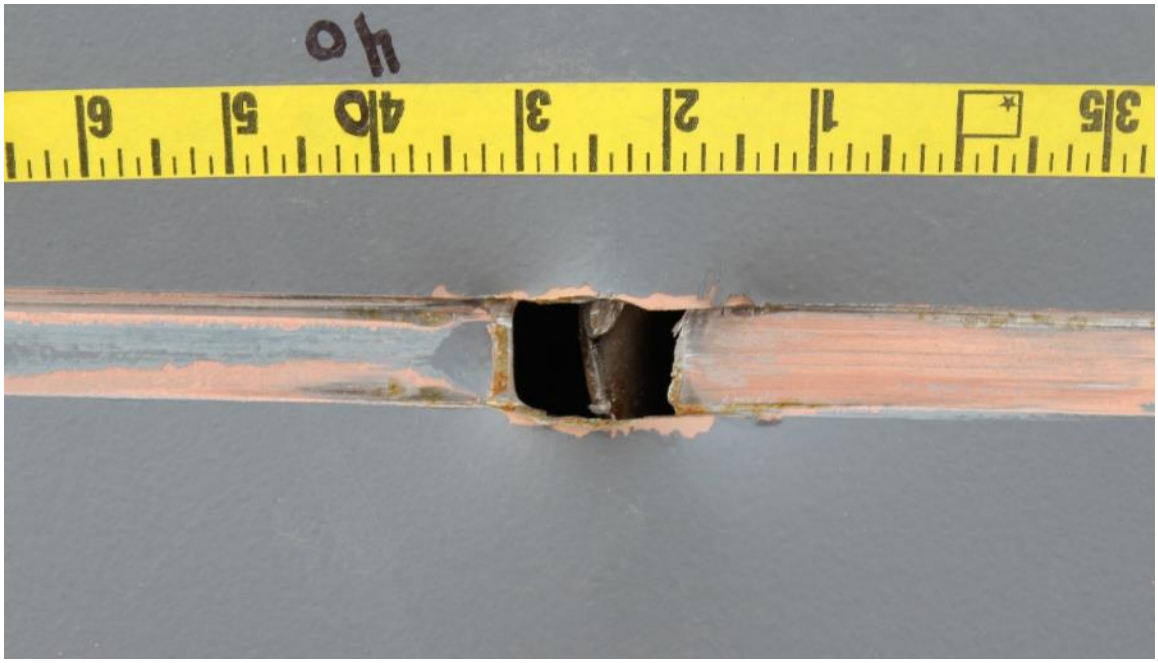

Figure 45. First Tear in Test 2 Fuel Tank

Figure 46. Second Tear in Test 2 Fuel Tank

4.2.1 Test 2 Measurements

Forces were measured at the point of load application at the end of the boxcar, and at the point of load reaction at the indenter. The test was initiated without the indenter in full contact with its load cell. As the raking continued, the fuel tank forced the indenter to contact the load cell. This occurred during the second push with the hydraulic cylinders at 16.8 inches of raking. Before the indenter contacted its load cell, that load cell gave a zero-force reading. Afterward, the load cell gave a reading which closely matched the force history of the boxcar load cell. The maximum force measured during this test was approximately 21,000 lbf and was measured at a raking distance of 20.3 inches. During the highest observed forces of the test, the indenter load cell measured a slightly higher force than the boxcar load cell. This result was unexpected, as the indenter load cell was reacting the force applied through the boxcar load cell. As such, the force measured from the indenter load cell was anticipated to be equal to or lower than the force measured at the boxcar load cell due to frictional and other losses between the application of load at the boxcar load cell and the indenter load cell. Figure 47 provides force measurements for Test 2.

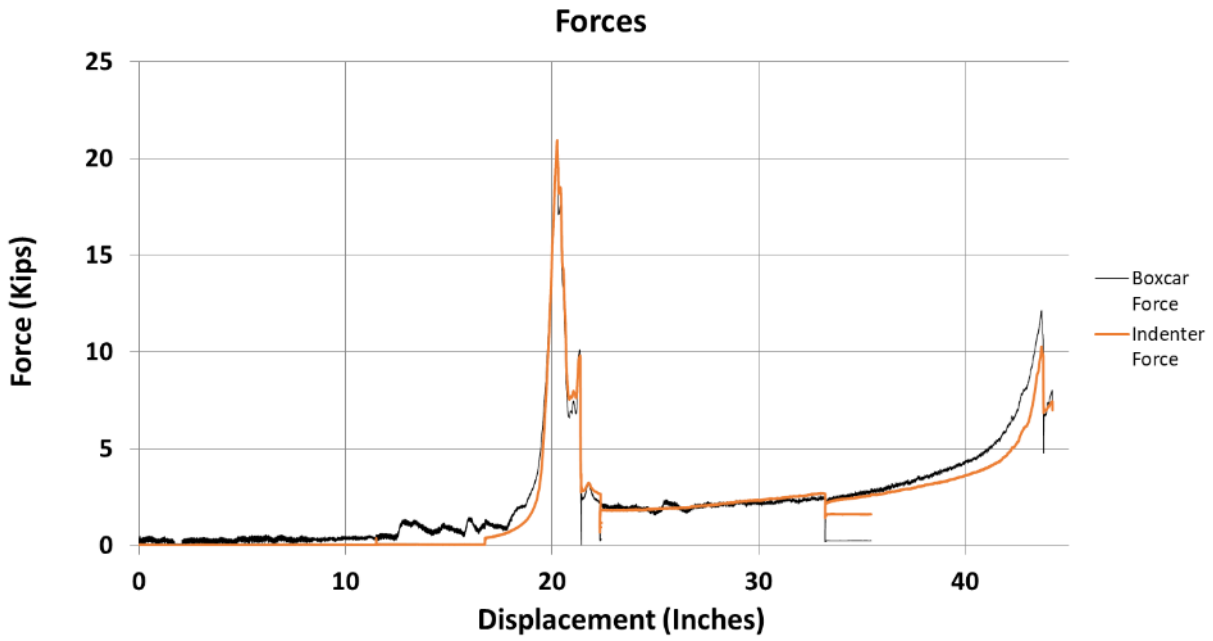

Figure 47. Test 2 Combined Force Measurements

Displacement of the boxcar and the fuel tank were measured relative to the ground. These measurements show similar displacement histories. Each measurement shows four separate periods of movement during the test of approximately 11 inches each, with a stationary period in-between. This represents the four strokes of the squeeze fixture's hydraulic cylinders with periods in-between to restrain the boxcar and install extenders. Figure 48 is a plot of the displacement measurements for this test.

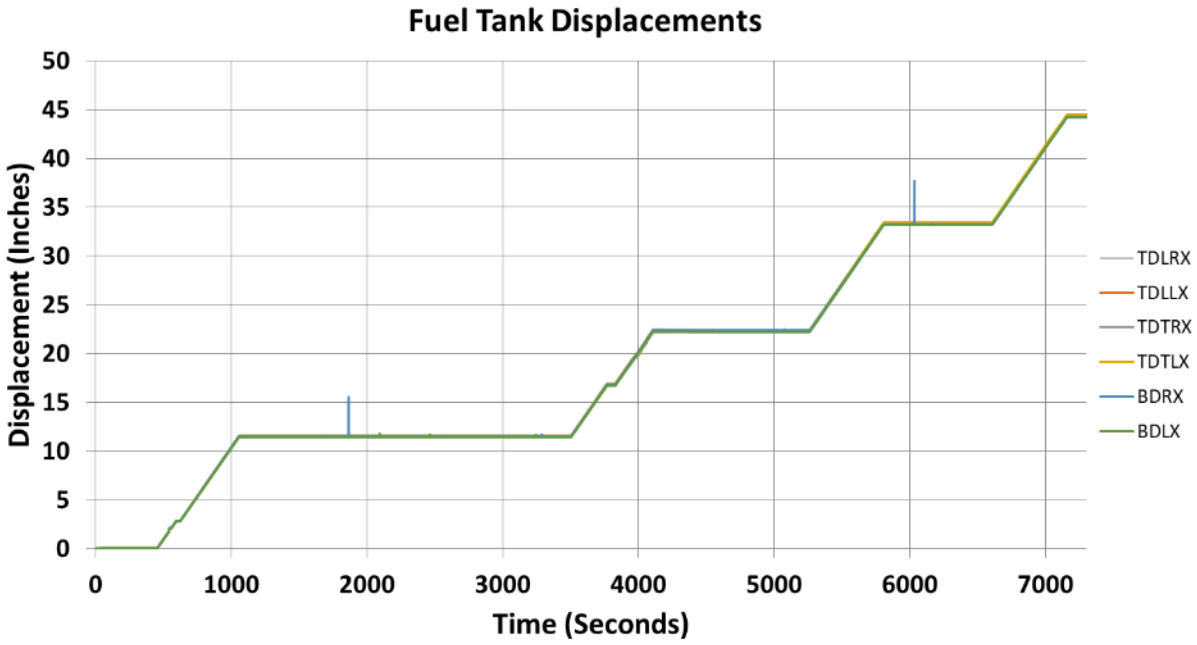

Figure 48. Test 2 Combined Displacement Measurements

After test completion, a laser scan was performed on the fuel tank in the area near the tear. This scan data revealed that the deformation of the tank's bottom sheet appeared to be minimal in areas not close to the tears. Due to the relatively small tears in this fuel tank, the tears are not well defined in the point cloud for this scan, see Figure 49.

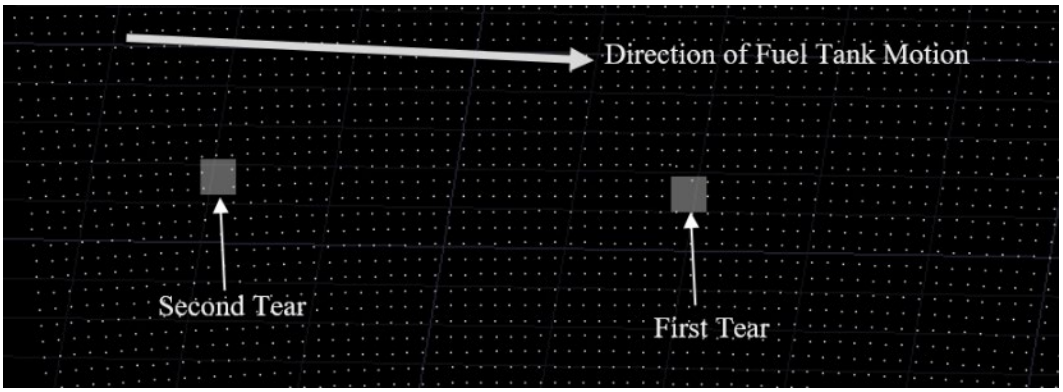

Figure 49. Test 2 Scan Point Cloud

4.3 Comparisons Between FE Models and Test Results

The key test results and model outcomes compared for each raking test are the global force-displacement response for each fuel tank, and the shape of the deformed tank.

4.3.1 Raking Test 1

Figure 50 shows a plot of reaction end forces versus displacement from the Pre-test 1 FE model and the test measurements. Both results are in good agreement over the first 2 inches of travel. Beyond that point, the test began to experience tearing while the model did not. Thus, the test forces dropped while the Pre-test 1 model forces continued to increase.

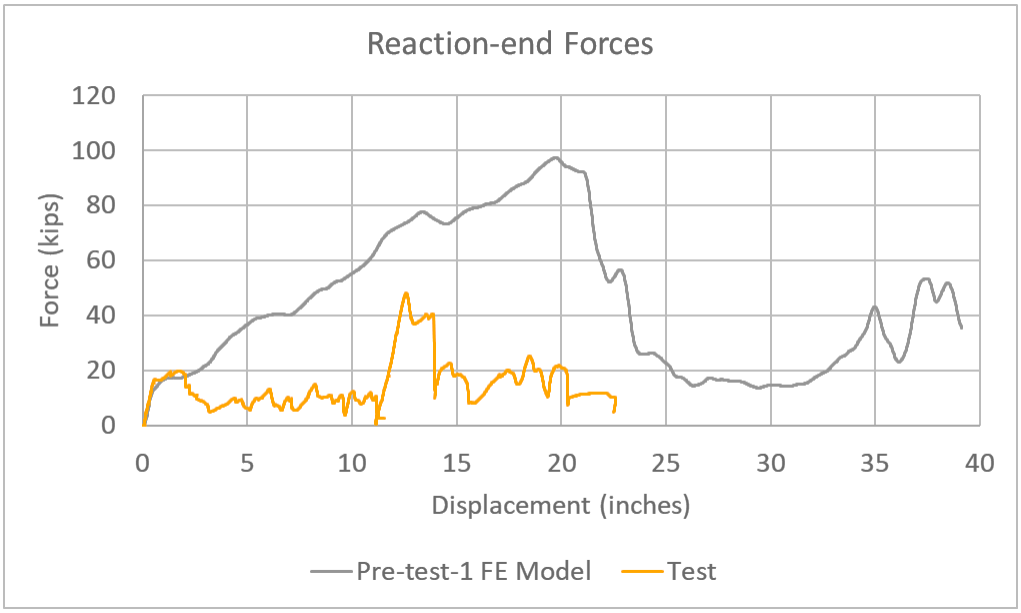

Figure 50. Pre-test 1 FE Model and Test Reaction-end Forces vs Displacement

Figure 51 shows the deformed shape of the Pre-test 1 FE model at the end of the simulation. Per this figure, the damage to the tank from this model is much more widespread than the highly-localized damage observed in the test (see Figure 38). Note that this figure is an inverted view of the fuel tank, with the indenter and its supporting hardware removed for clarity.

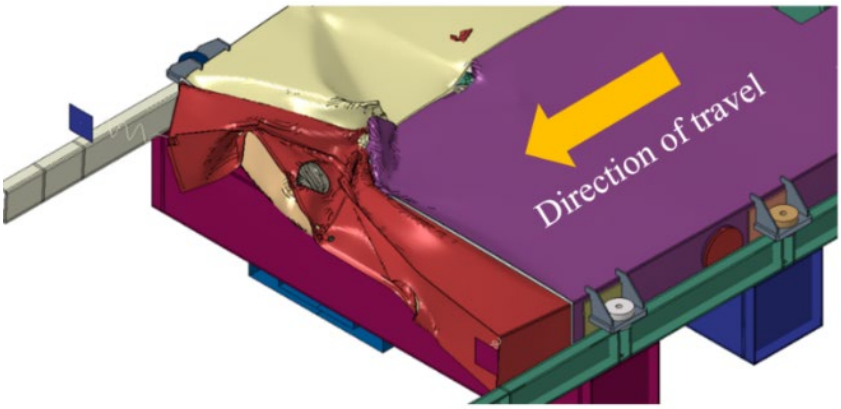

Figure 51. Deformed Shape of Pre-test 1 FE Model

It is apparent that the Pre-test 1 FE model over-predicted the forces expected to be imparted to the fuel tank. This was largely due to the Pre-test 1 FE model not experiencing puncture initiation at displacement of approximately 2 inches, where the test did begin to experience such tearing. Thus, following the test, adjustments were made to the Pre-test 1 FE model. These adjustments included refining the mesh size near the area of contact between the fuel tank and the indenter and adjusting the material failure model to correspond to using finer elements in the failure zone. Figure 52 shows the area where the indenter contacts the edge of the tank in the post-test FE model. Note that this image has been inverted, looking down on the bottom of the fuel tank.

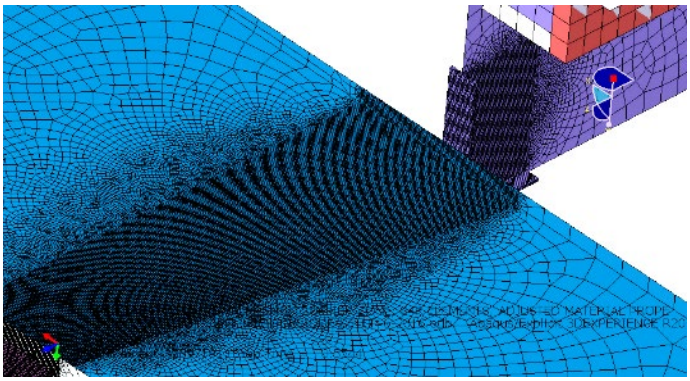

Figure 52. Image from Model Showing Refined Mesh (inverted view)

Figure 53 shows the extent of the tearing to the end plate and bottom sheet from the post-test FE model. Note that the model terminated after approximately 15 inches of travel, while the test continued through 21 inches of travel. This termination is associated with the large amount of deformation and element failure which occurred in the model by this point. The tearing shown in Figure 53 exhibits some similarities to the tearing observed in the test (see Figure 38 and Figure 43). In general, the FE model exhibited more widespread damage and less-clean tearing of the bottom sheet than what was observed in the test.

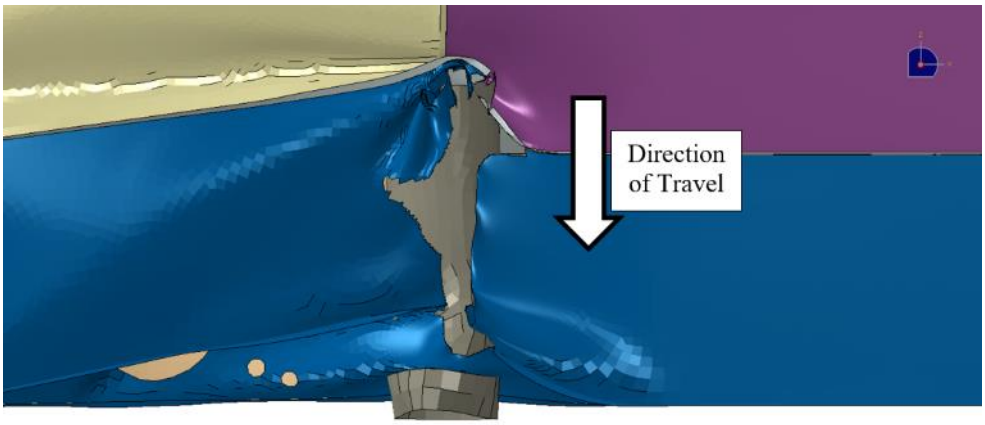

Figure 53. Deformed Shape of Post-test FE Model

Figure 54 shows a comparison of the test measurements and corresponding results from the FEA. For both the test and the FEA, the indenter force is plotted against the travel of the fuel tank. The initial tear represents the initiation of puncture to the tank, while continued movement of the tank past the indenter is damage propagation. The model underestimates the peak force required to initially puncture the DMU fuel tank. This part of the test data is highlighted with a red box.

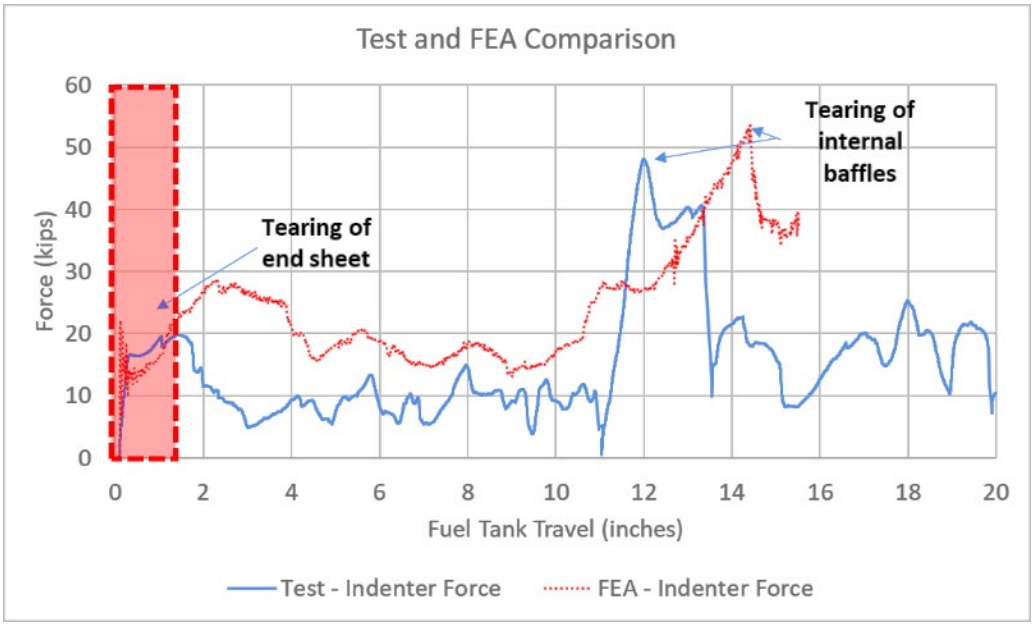

Figure 54. Test and Post-test Model Comparison

After the initial tearing, the model tends to overestimate the force necessary to propagate the tear. Qualitatively, the model exhibits a similar response shape to the test, with an initial tear followed by a drop in force. Subsequently, the force level begins to climb again as the internal baffle passes over the indenter. Quantitatively, the model's estimated force magnitudes and displacement at which the force subsequently climbed did not exhibit close agreement. It should be noted that the global peak force associated with internal baffle tearing agreed to within 15 percent.

There are several possible sources of discrepancy between test and model. The material model chosen for damage initiation may not be as well suited to capturing the continued propagation as

it is to capture the initial tearing. In addition, the damage mode is a highly complicated combination of folding, shearing, and ultimately tearing of the material. Further mesh refinement or exploration of additional material failure modeling strategies may be necessary to better capture the failure modes observed in the test.

4.3.2 Raking Test 2

Figure 55 shows a comparison between deformed shape from the Pre-test 2 FE model and the test results. The model estimated a similar pattern of striation in the bottom sloped surface of the fuel tank to what occurred in the test. Two distinct locations of material failure are seen in both the model and the test results.

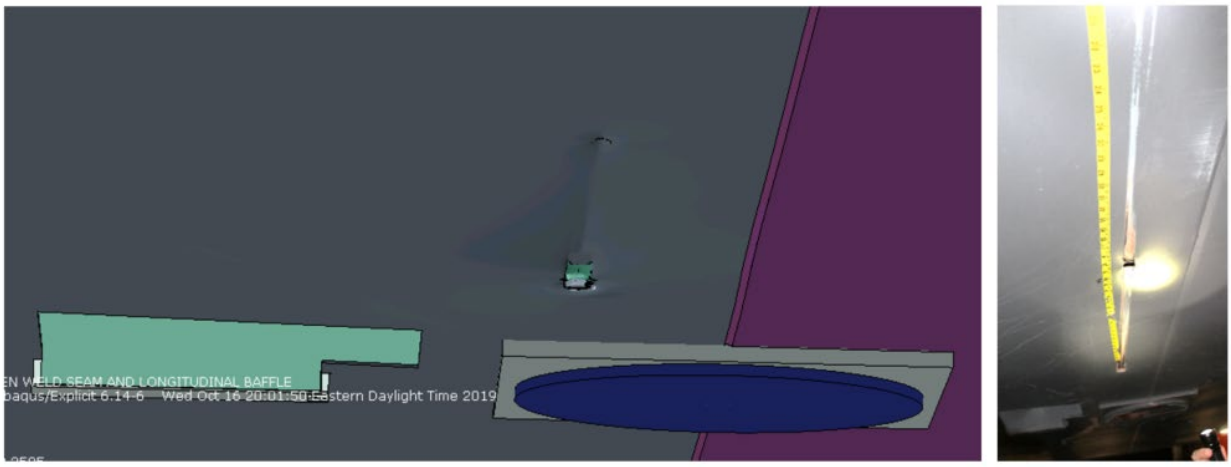

Figure 55. Comparison of Fuel Tank Deformation in Pre-test 2 FEA and Test

Figure 56 shows a plot of the force versus longitudinal displacement for both the test and the Pre-test 2 model. This pre-test model assumed that the indenter would be positioned such that it made initial contact with the bottom of the fuel tank immediately. However, as seen in this figure, the test measurements revealed that the force did not increase immediately during the test, but rather required a significant amount of "slack" longitudinal travel to occur before the indenter load cell began to register a force.

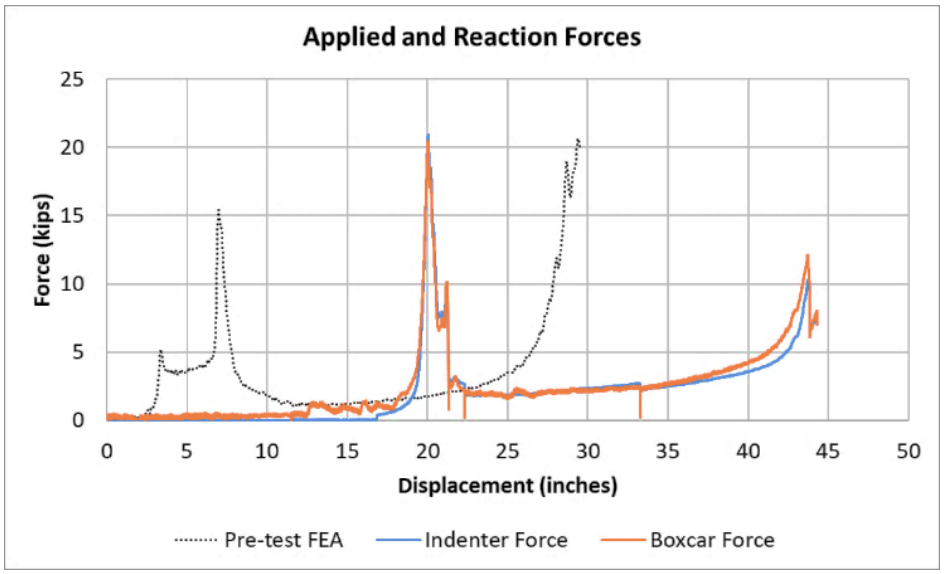

Figure 56. Comparison of Test Data and Pre-test 2 FEA (unshifted results)

Following the test, the Pre-test 2 FEA result was shifted laterally by approximately 15 inches. This displacement corresponds to a distance midway between where the boxcar force (i.e., the live end) and the indenter force (i.e., the reaction end) experience an appreciable increase. Figure 57 shows the shifted Pre-test 2 FE results. The Pre-test 2 model predicted a relatively low force of less than 2,000 lbf until about 18 inches of shifted displacement. The force then increased to a peak of 15,000 lbf to 20,000 lbf and drops off within 5 inches of travel, indicating the first puncture location. The load then reached a plateau at about 2,500 lbf for 20 inches of travel until a second peak occurred at about 44 inches in both the test and the shifted model.

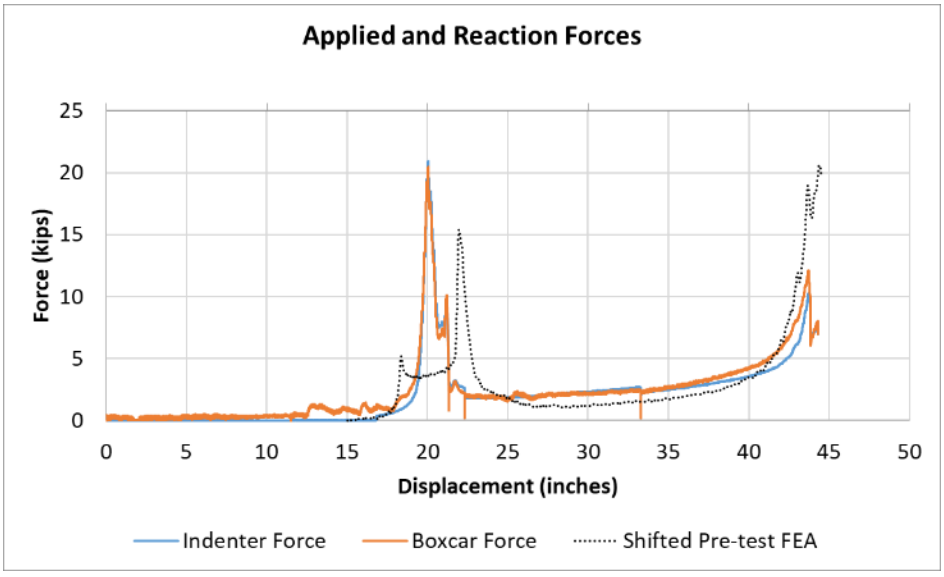

Figure 57. Comparison of Test Data and Pre-test FEA (shifted results)

In general, the model captured the response of the fuel tank in raking Test 2. Similar to the results of raking Test 1, the force levels and the location of the peak displacements are not in perfect agreement with the test measurements.

5. Conclusion

TTCI performed two raking tests on DMU fuel tanks using an indenter shaped similarly to a broken rail. The first raking test positioned the indenter against the fuel tank's end plate, with 2 inches of overlap between the top of the indenter and the bottom of the end plate. The indenter scraped the surface of a previously tested DMU fuel tank for 22.6 inches and achieved a maximum force of 51,000 lbf. The raking caused a tear to form in the surface of the fuel tank for the full 22.6 inches of travel. The second test positioned the indenter against the sloped bottom sheet of a fuel tank. The indenter scraped the surface of a newly built DMU fuel tank for 44.2 inches and achieved a maximum force of 21,000 lbf. Although the indenter caused deformation in the fuel tank's bottom sheet for the entire 44.2 inches of travel, the tank experienced tearing only near internal longitudinal baffles. These results indicate that lower overall forces are required to tear these DMU fuel tanks along their bottom sheets, compared to puncturing the end sheets. In addition, the overall deformation caused by the rakings was small and localized to the area near contact with the penetrating object. The results of the FEA models show that there was good general agreement in estimating the overall behavior of the fuel tank under the two test cases.

Research on measuring fuel tank performance in raking scenarios is the second phase of FRA's fuel tank research program. Research into raking behavior of thin plate metal structures is challenging to find, with the exception of a few studies on marine ships impacting underwater objects [14] [15]. The modeling developed in the fuel tank program uses material failure criterion developed from tank car impact tests. The series of blunt impact tests of a variety of fuel tanks helped develop that theory for fuel tank testing. The raking modeling efforts use the models developed for assessing the blunt impact tests to predict the behavior of the fuel tanks in the raking tests. The results of the two raking tests show that the FEA is a reasonable tool for estimating the performance of the fuel tanks under certain loading conditions. However, there are several significant challenges to using FEA to predict the tearing behavior to fuel tanks. The impact response appears to be quite sensitive to the initial overlap between the striking and struck objects. The models require an especially fine mesh over a large area to capture tear propagation. Material models that have worked reasonably well in past research programs for estimating the failure behavior of blunt impact behaviors did not provide a high level of agreement with the shear-dominated raking loading. Additional model sensitivity and material failure characterization studies are recommended if additional raking impact analyses are planned.

The raking tests provided data on a common loading condition that has been observed in numerous locomotive fuel tank puncture incidents. A notable observation in the overall behavior of fuel tanks in the raking scenario is the influence of internal baffles. Similar to what has been observed in the blunt impact tests, the location and connection details of baffles along the impacted surface of the tank influence the force-deflection behavior of the fuel tanks. A second observation can be made on how the design of the fuel tank dimensions can influence the exposure to threats. The DMU tests features a bottom surface that slopes down to a drain pan at the center. The lowest point of the fuel tank bottom is lower than the lowest point of the end plate. While fuel tank end plates in the North American market are typically designed to be thicker to endure a side impact, the thinner bottom surface of a DMU fuel tank may be exposed to a side impact, as seen in Test 2.

6. References

1. Gorhum, T., Carolan, M., Rakoczy, P., Jacobsen, K., Eshraghi, S., and Shurland, M., "Blunt Impact Tests of Diesel Multiple Unit Fuel Tank," Technical Report No. DOT/FRA/ORD-18/22, Washington, DC: U.S. Department of Transportation, Federal Railroad Administration, July 2018.
2. Jacobsen, K., "Fuel Tank Crashworthiness: Loading Scenarios," *Proceedings of the ASME/ASCE/IEEE 2011 Joint Rail Conference*, Paper No. JRC2011-56077, Pueblo, CO, March 2011.
3. Carolan, M., Rakoczy, P., and Jacobsen, K., "Blunt Impact Tests of Retired Passenger Locomotive Fuel Tanks," Technical Report No. DOT/FRA/ORD-17/11, Washington, DC: U.S. Department of Transportation, Federal Railroad Administration, August 16, 2017.
4. Jacobsen, K., Carolan, M., and Shurland, M., "Passenger Locomotive Fuel Tank Integrity Research," *Proceedings of the 4th International Conference on Fires in Vehicles FIVE 2016*, October 2016.
5. Jacobsen, K., Carolan, M., Perlman, A. B., "Conventional Fuel Tank Blunt Impact Tests: Test and Analysis Results," *Proceedings of the 2014 Joint Rail Conference*, Paper No. JRC2014-3786, Colorado Springs, CO, April 2014.
6. Jacobsen, K., Llana, P., Carolan, M., and Sullivan, L., "Fuel Tank Integrity Research: Fuel Tank Analyses and Test Plans," *Proceedings of 2013 ASME/IEEE/ASCE Joint Rail Conference*, Paper No. JRC2013-2425, Knoxville, TN, April 2013.
7. Jacobsen, K., Carolan, M., and Llana, P., "Test Requirements of Locomotive Fuel Tank Blunt Impact Tests," *Proceedings of the 2013 ASME Rail Transportation Division Fall Technical Conference*, Paper No. RTDF2013-4701, Altoona, PA, October 2013.
8. Jacobsen, K., Carolan, M., "Results of a Conventional Fuel Tank Blunt Impact Test," *Proceedings of the 2015 Joint Rail Conference*, Paper No. JRC2015-5759, San Jose, CA, March 2015.
9. Jacobsen, K., Carolan, M., "Results of a Diesel Multiple Unit Fuel Tank Blunt Impact Test," *Proceedings of the 2017 Joint Rail Conference*, Paper No. JRC2017-2248, Philadelphia, PA, April 2017.
10. Abaqus version 6.14. Dassault Systems Simulia Corp, Providence, RI, 2014.
11. Matweb, ASTM A514 Steel, Grade B, plate thickness < 19mm [Online].
12. Piedmont Plastics, Fluoropolymer Spec Chart [Online].
13. Engineering ToolBox, *Rolling Resistance* [Online], 2008.
14. Wierzbicki, T., "Concertina Tearing of Metal Plates," *International Journal of Solids and Structures, 32*(19), pp 2923–2943, 1995.
15. Wang, G., Ohtsubo, H., and Liu, D., "A Simple Method for Predicting the Grounding Strength of Ships," *Journal of Ship Research*, *41*(3), September 1997, pp 241–247.

Appendix A.
Test 1 Data

Figures A1 through A9 contain raw data from the first fuel tank raking test.

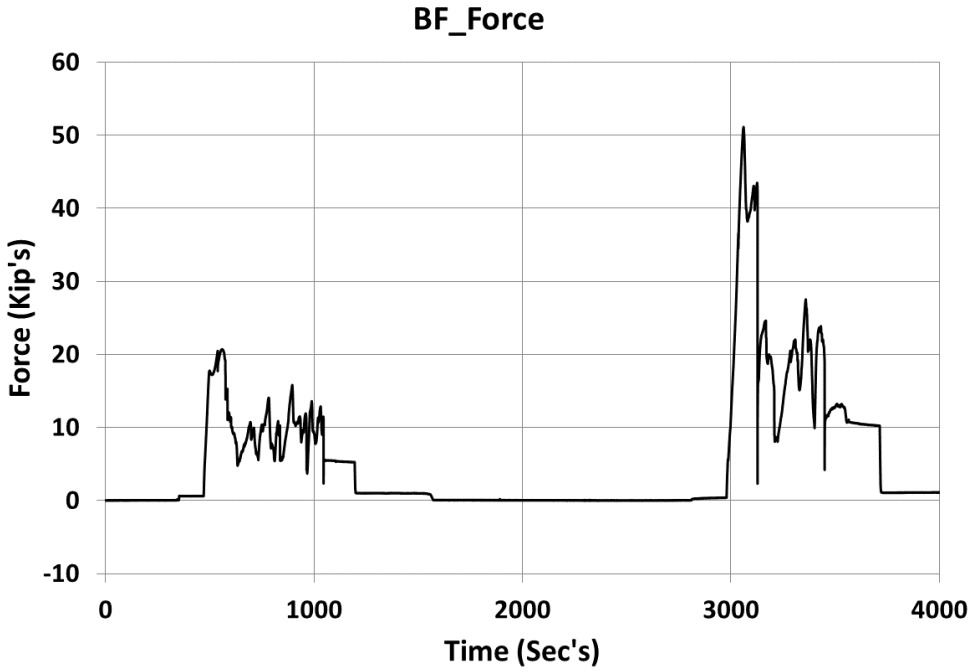

Figure A1. BF Force Data

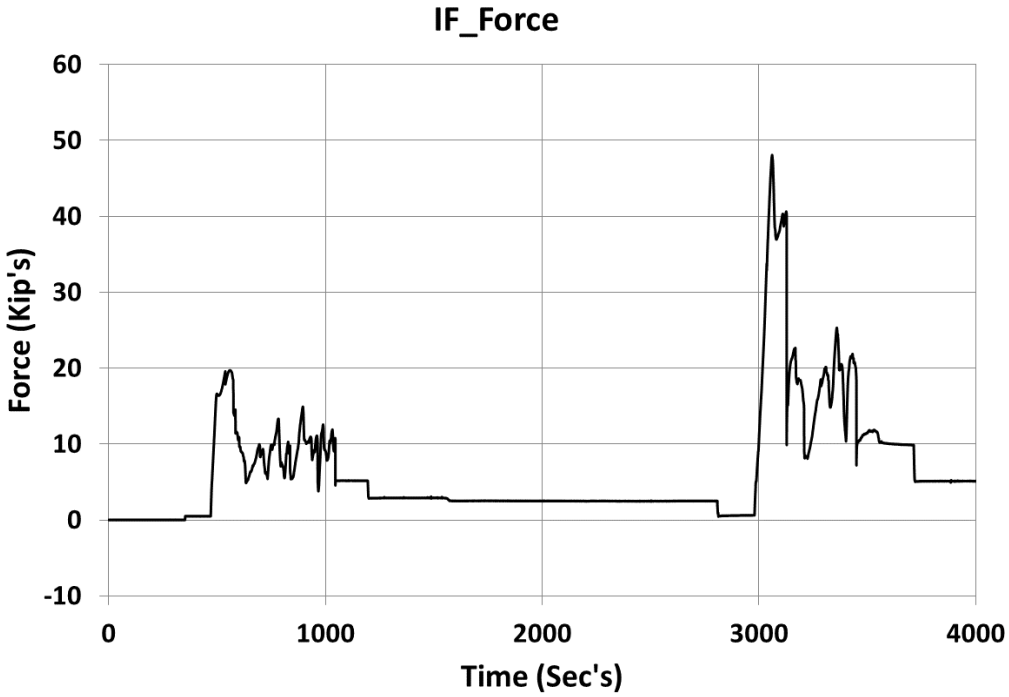

Figure A2. IF Force Data

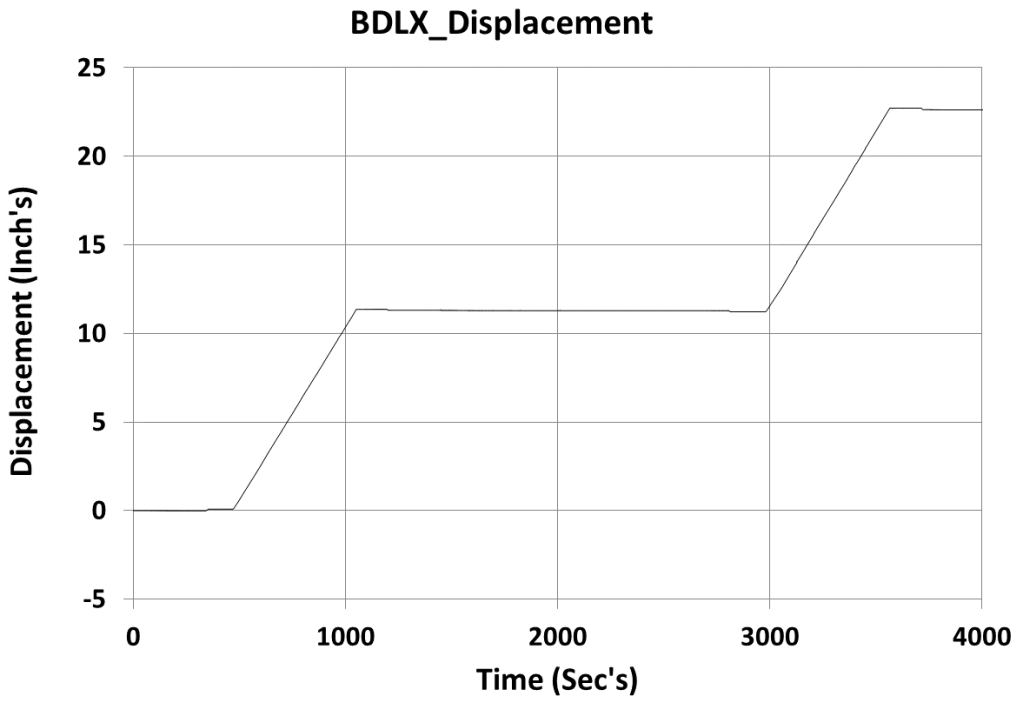

Figure A3. BDLX Displacement Data

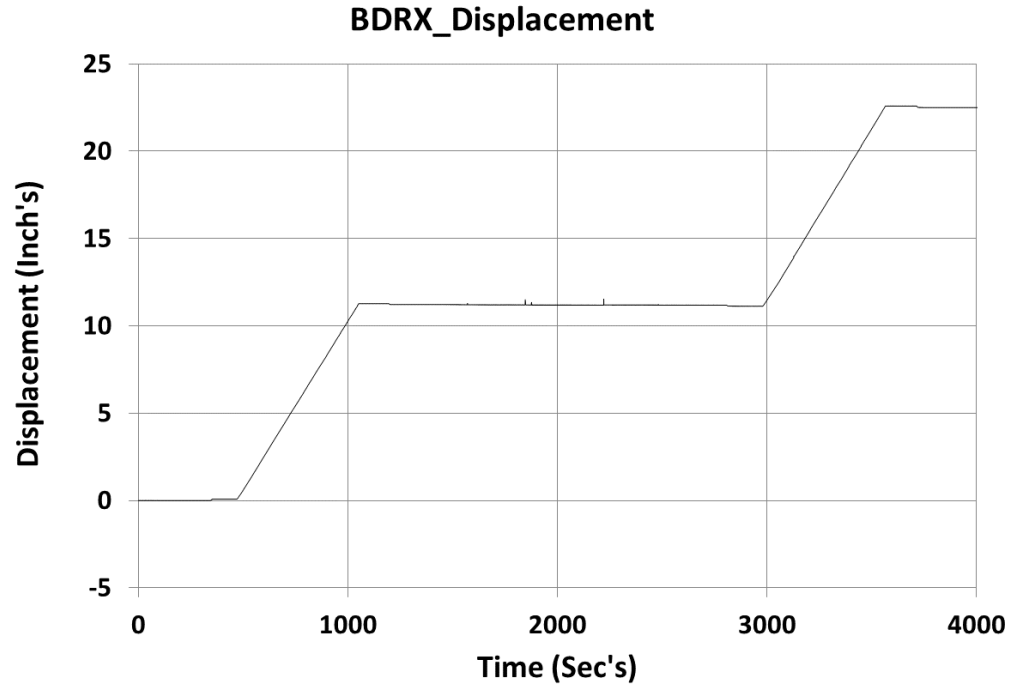

Figure A4. BDRX Displacement Data

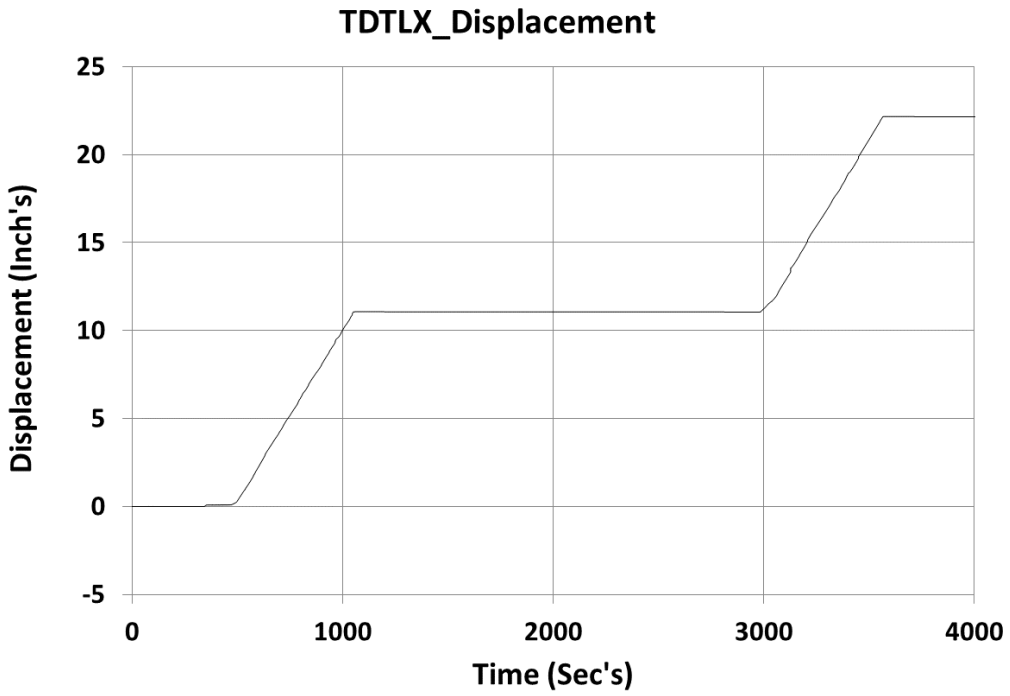

Figure A5. TDTLX Displacement Data

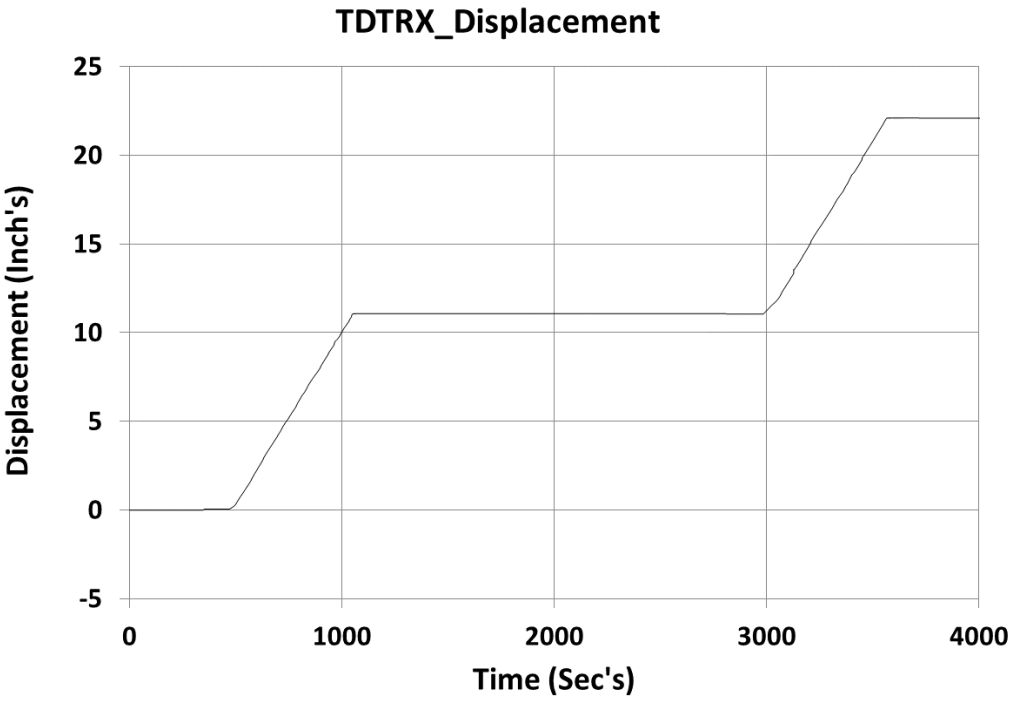

Figure A6. TDTRX Displacement Data

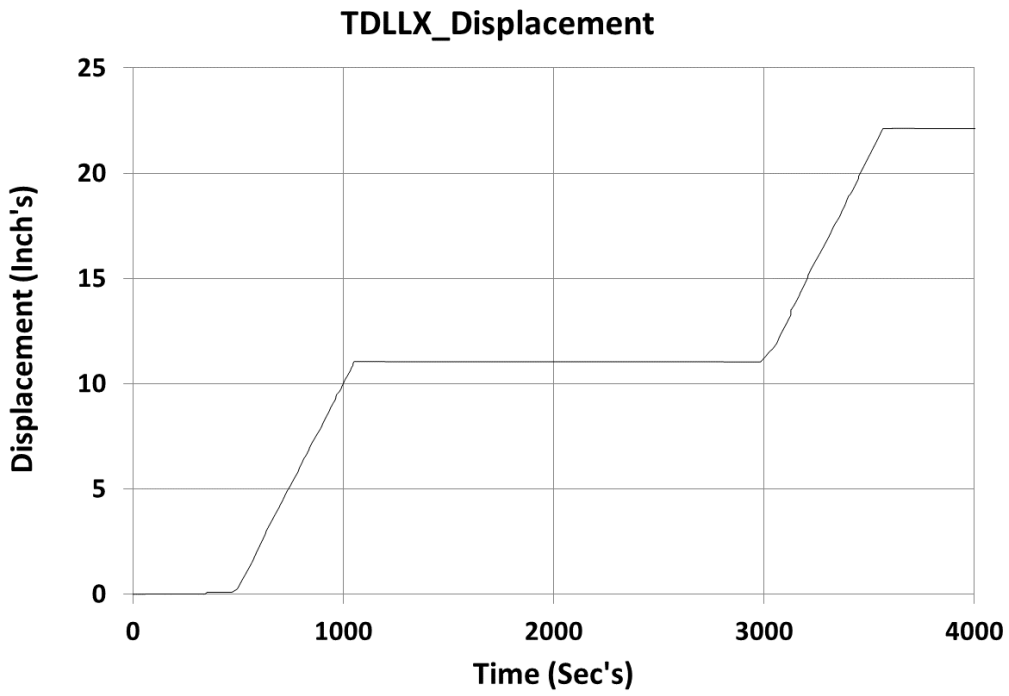

Figure A7. TDLLX Displacement Data

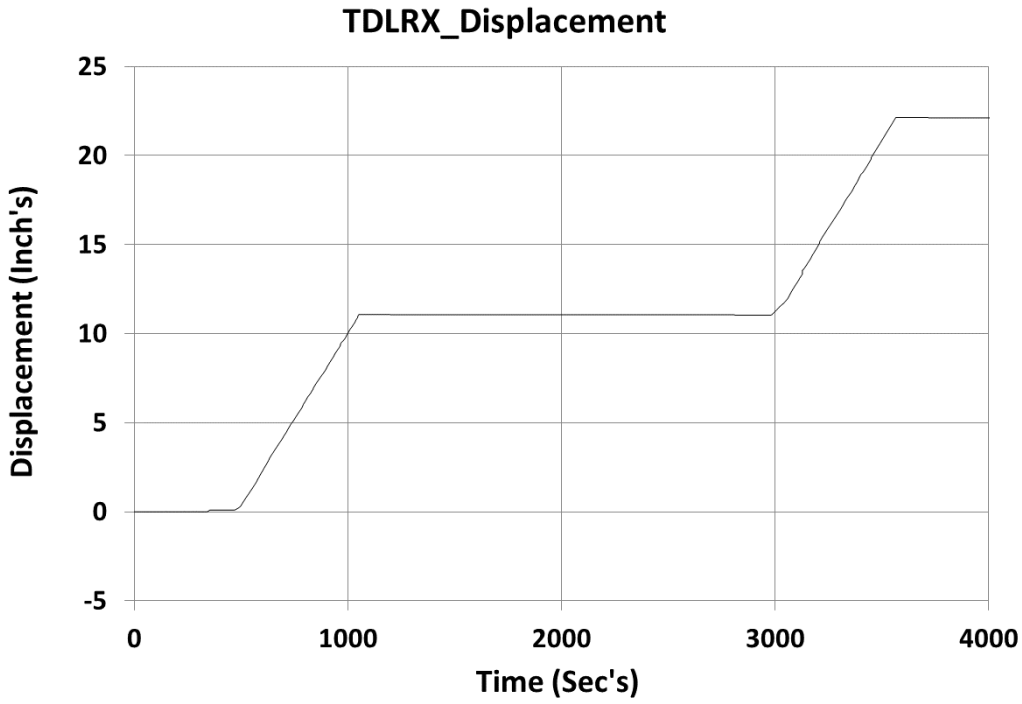

Figure A8. TDLRX Displacement Data

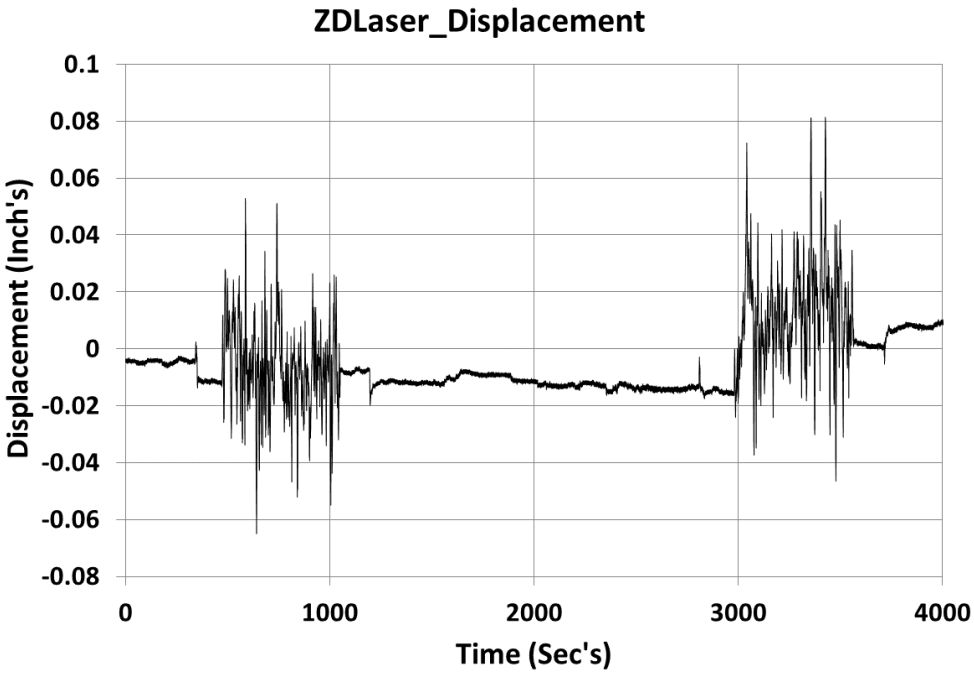

Figure A9. ZDLaser Displacement Data

Appendix B: Test 2 Data

Figures B1 through B9 contain raw data from the second fuel tank raking test.

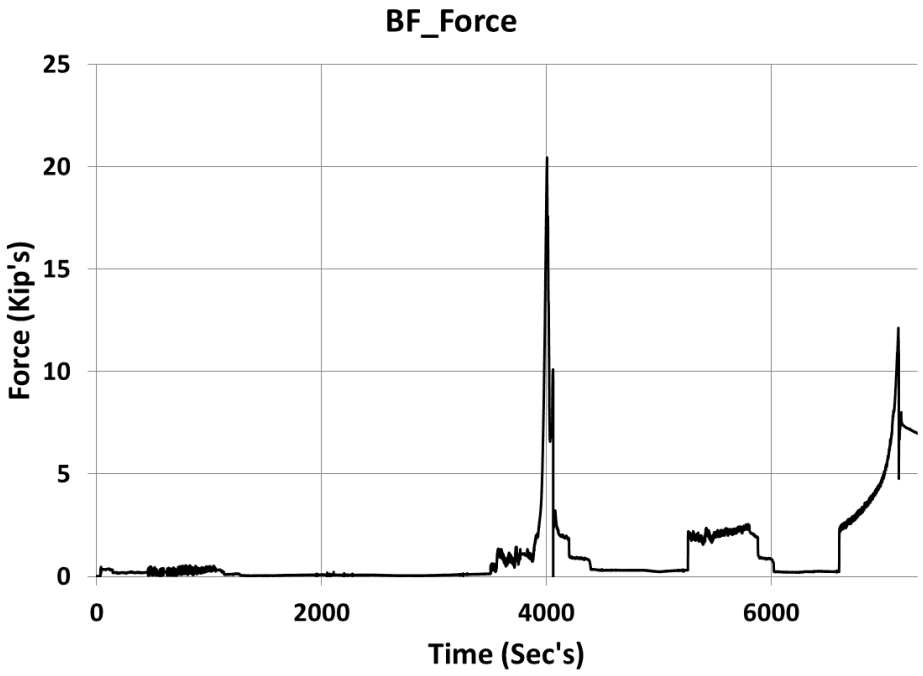

Figure B1. BF Force Data

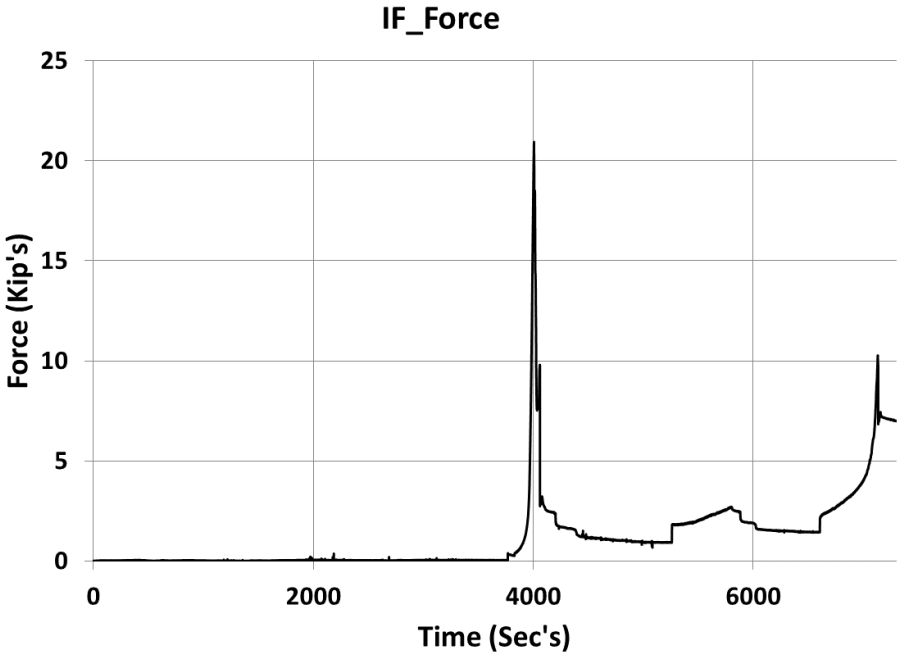

Figure B2. IF Force Data

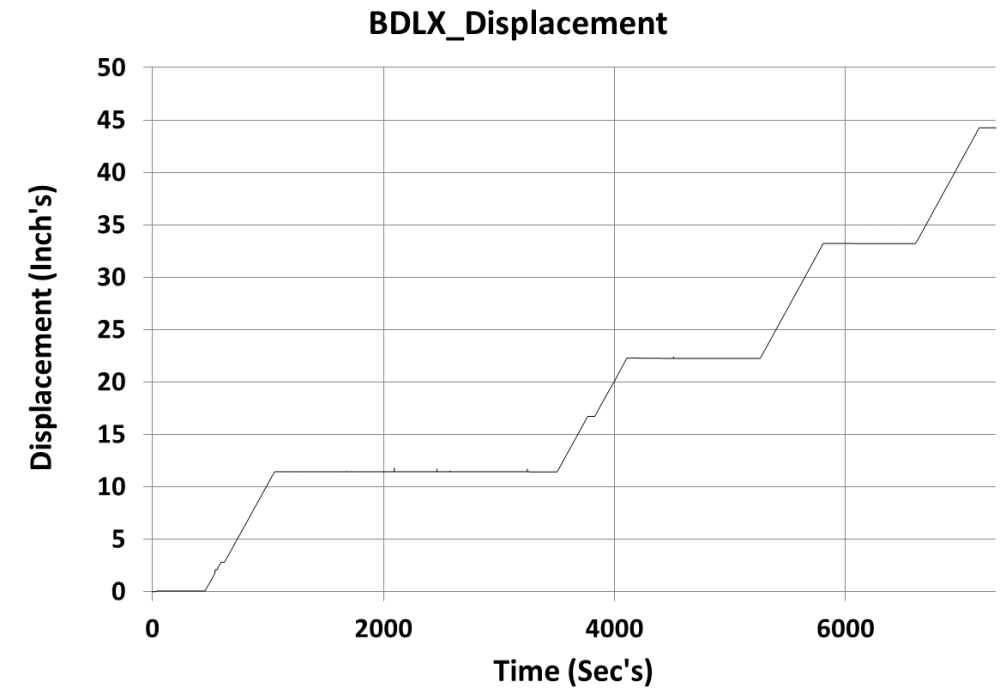

Figure B3. BDLX Displacement Data

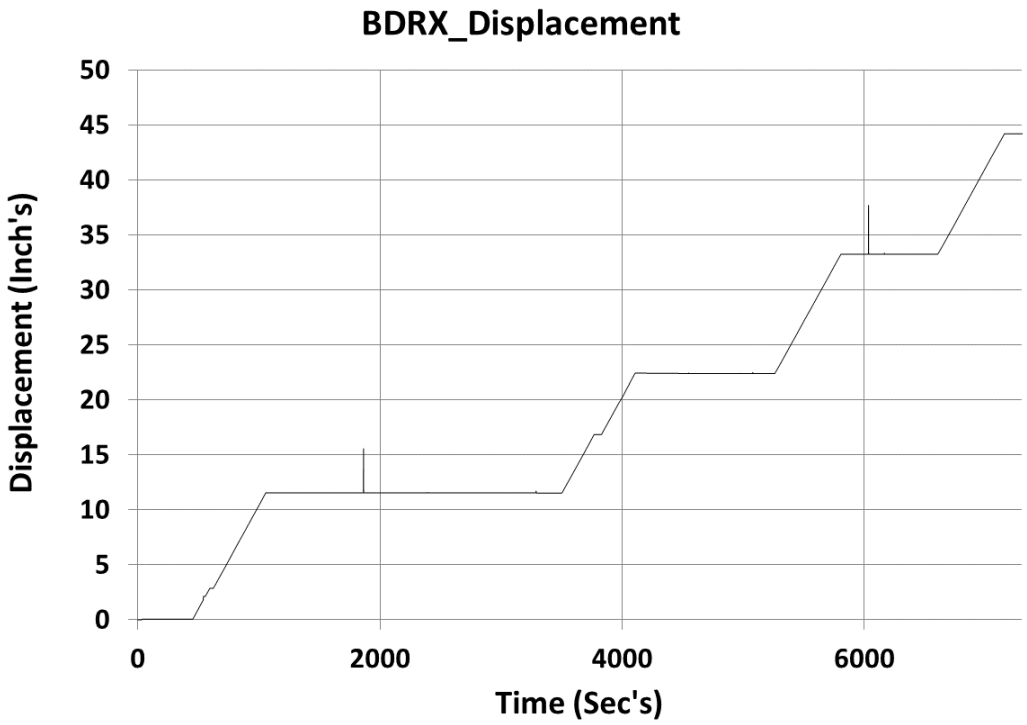

Figure B4. BDRX Displacement Data

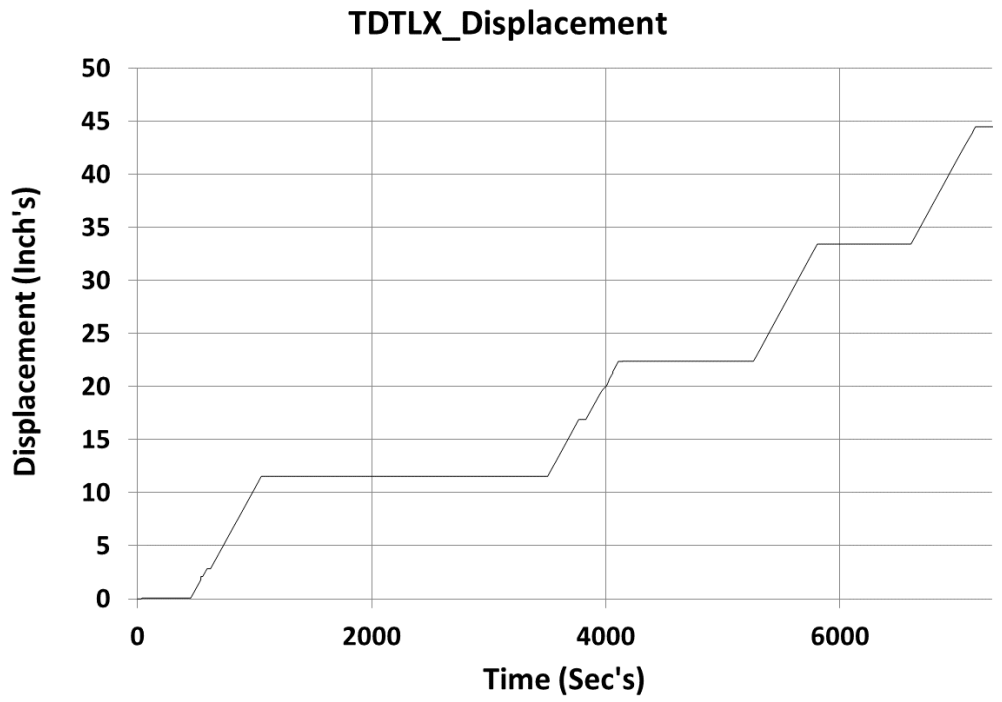

Figure B5. TDTLX Displacement Data

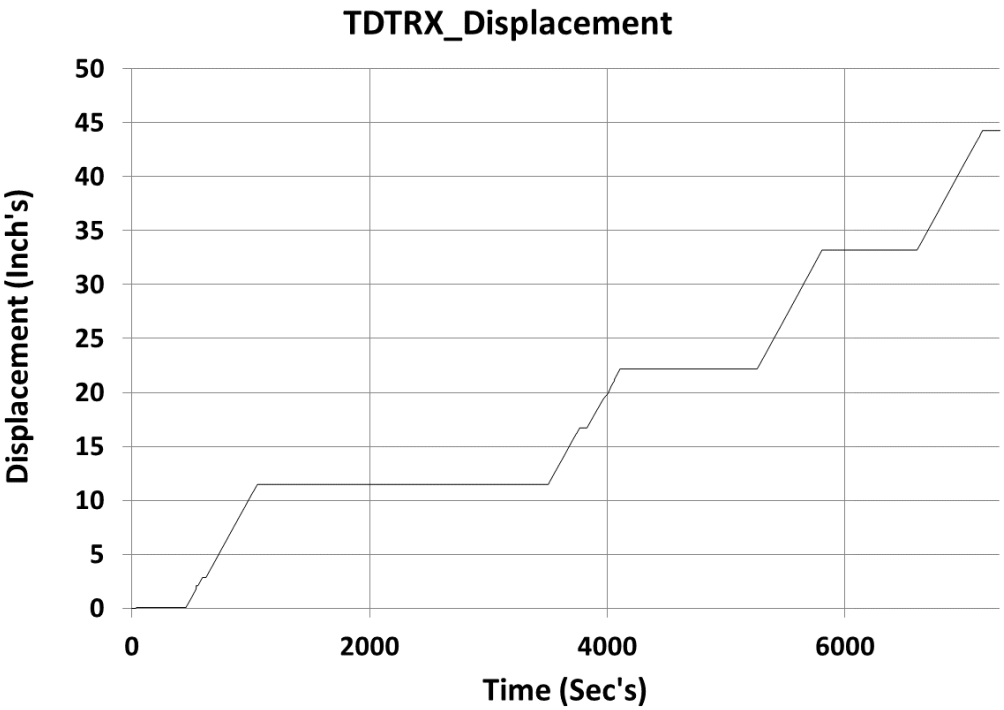

Figure B6. TDTRX Displacement Data

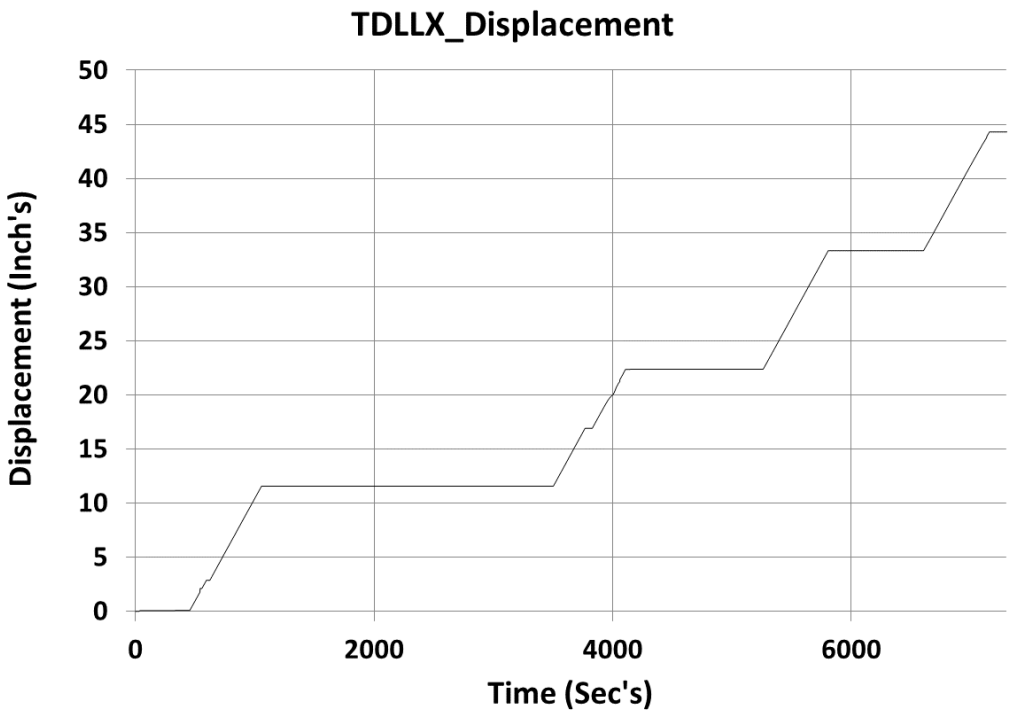

Figure B7. TDLLX Displacement Data

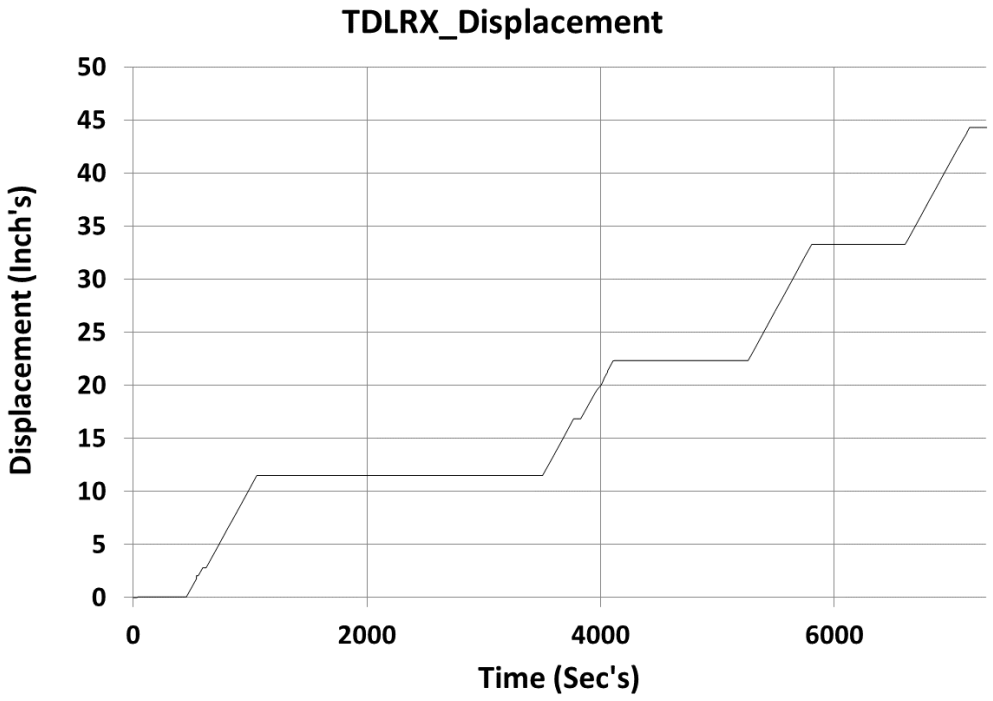

Figure B8. TDLRX Displacement Data

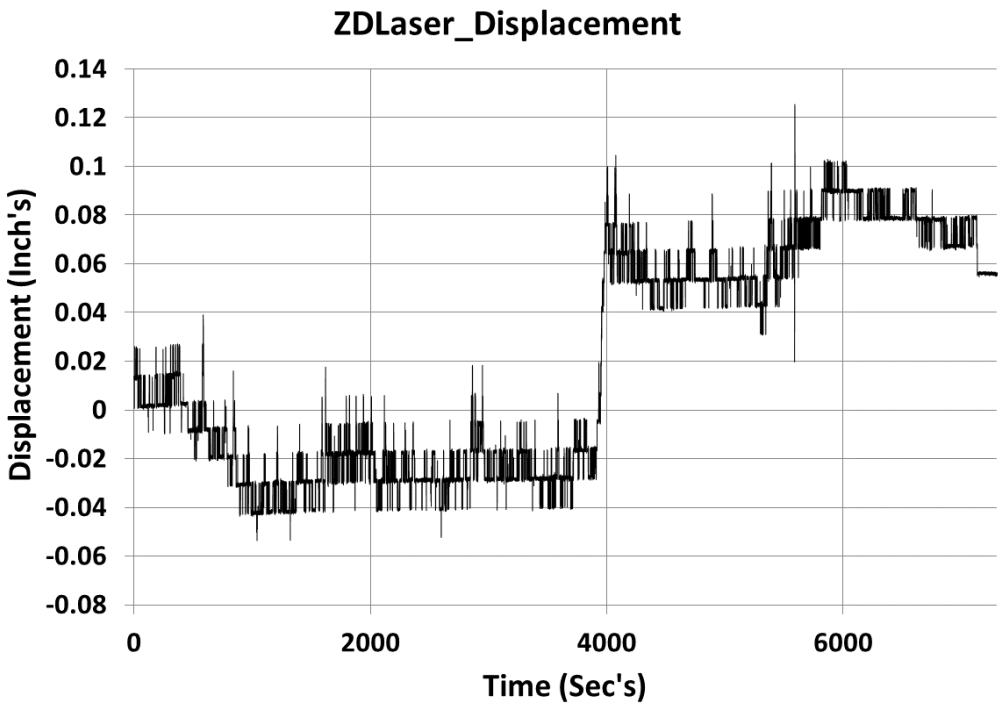

Figure B9. ZDLaser Displacement Data

Abbreviations and Acronyms

ACRONYMS	EXPLANATION
BF	Boxcar Force
CAD	Computer-Aided Design
DOF	Degrees of Freedom
DMU	Diesel Multiple Unit
FRA	Federal Railroad Administration
FE	Finite Element
FEA	Finite Element Analysis
IF	Indenter Force
LIDAR	Light Detection and Ranging
ms	Milliseconds
MPC	Multi-Point Constraint
PTFE	Polytetrafluoroethylene
lbf	Pound-force
TTC	Transportation Technology Center
TTCI	Transportation Technology Center, Inc.
Volpe	Volpe National Transportation Systems Center